Submitted to Sedimentary Geology

The subaqueous landslide cycle in south-central Chilean lakes: the role of tephra, slope gradient and repeated seismic shaking

Moernaut, J.[a*], Van Daele, M.[b], Heirman, K.[b,1], Wiemer, G.[c], Molenaar, A.[a], Vandorpe, T.[d], Melnick, D.[e], Hajdas, I.[f], Pino, M.[e], Urrutia, R.[g], De Batist, M.[b]

[a] Institute of Geology, University of Innsbruck, Innrain 52, Innsbruck, Austria

[b] Renard Centre of Marine Geology, Ghent University, Krijgslaan 281(S8), Ghent, Belgium

[c] MARUM - Centre for Marine Environmental Sciences, University of Bremen, Leobener Strasse 8, Bremen, Germany

[d] Flanders Marine Institute, Wandelaarkaai 7, Oostende, Belgium

[e] Instituto de Ciencias de la Tierra and TAQUACH, Universidad Austral de Chile, Campus Isla Teja, Valdivia, Chile

[f] Laboratory of Ion Beam Physics, ETH Zürich, Campus Hönggerberg, Zürich, Switzerland

[g] Centro EULA-Chile and Centro CRHIAM, Universidad de Concepción, Casilla 160-C, Concepción, Chile

[1] present address: Division of Ecological and Earth Sciences, UNESCO Earth Sciences and Geo-hazards Risk Reduction, Place de Fontenoy, Paris, France

*Corresponding author: Jasper.Moernaut@uibk.ac.at

Abstract

Subaqueous landslides are common features at active and passive ocean margins, in fjords and lakes. They can develop on very gentle slope gradients (<2°) and the presence of sandy tephra layers seems to facilitate the development of translational failure. Despite numerous investigations, it remains elusive how different slope preconditioning factors act and interact over time and how different triggering mechanisms can lead to slope failure. In settings of low to moderate seismicity, stratigraphic sequences with sublacustrine mass-transport deposits (MTDs) have successfully been used for constructing prehistorical earthquake catalogues. In high seismicity areas, it is inferred that not all strong earthquakes succeed in triggering landslides on the investigated slope segments, and MTD records do not fully represent their complete recurrence pattern. Here, we present the spatio-temporal distribution of MTDs in two large glacigenic Chilean lakes (Villarrica and Calafquén) based on a detailed seismic-stratigraphic analysis and several radiocarbon-dated piston cores (up to 14 m long). We find a strong influence of slope gradient on the occurrence and volume of landslide

events; i.e. most (small) landslides take place on slopes of 5-20°, whereas the few large (potentially tsunamigenic) landslides exclusively occur on slopes of <4°. Liquefaction of sandy tephra layers facilitates the development of thin (<0.5 m) in-situ deformations during earthquake shaking. When sandy tephra layers get progressively buried, liquefaction becomes unlikely, but repeated excess pore pressure transfer to overlying units facilitates the development of translational sliding. The occurrence of voluminous landslides seems to follow a "landslide cycle" which starts with the deposition of a tephra layer and the development of in-situ deformations directly on top. Once the slope sequence reaches a critical thickness, the end of the cycle is indicated by incipient scarp development, and subsequent major sliding event(s). The duration of the landslide cycle is defined by the rate of gradual sedimentation, but may be affected by sudden geological events (e.g., volcanic eruptions), expediting the end of the cycle. Despite the many methodological challenges inherent to the construction of a MTD stratigraphy, we propose that well-dated multiple MTD events can be used as positive evidence to strengthen and specify the regional paleoseismic record, concerning the largest events in a high-seismicity region. This method is most successful when targeting the base of relatively steep slopes (5-20°) with frequent, minor landsliding, and complementing this with seismic-stratigraphic analysis of fluid-escape features and correlation with distal turbidite records.

Keywords: subaqueous landslides; paleoseismology; mass-transport deposit; Chile; turbidite

1. Introduction

Subaqueous landslides are important sediment-transport processes, reshaping passive and active ocean margins (McAdoo et al., 2000; Hühnerbach et al., 2004; Talling et al., 2014; Moscardelli and Wood, 2016; Clare et al., 2018), marine coastal settings (Mosher et al., 2004), fjords (Parsons et al., 2014; Bellwald et al., 2016) and lake basins (Moernaut and De Batist, 2011; Sammartini et al., in press). Due to their potential to trigger large tsunamis, they can constitute significant geohazards for coastal populations and infrastructure (Tappin et al., 2001). They can transform into long-runout turbidity currents that break seafloor telecommunication cables (Pope et al., 2017). Many processes have been proposed that can lead to subaqueous landslides (Locat and Lee, 2002), including long-term slope preconditioning factors (e.g., weak layers, pore water overpressure, oversteepened slopes) and short-term triggering mechanisms (e.g. earthquakes, wave loading, and sudden fluid seepage). Accurate testing is difficult as subaqueous landslides are hard to monitor and only few landslides are sampled and accurately dated, making comparisons between landslide occurrence and external forcing factors a difficult task (Urlaub et al., 2013).

In terms of preconditioning factors, one of the most remarkable features of subaqueous landslides is that they can occur on slope gradients of only a few degrees, a situation which is almost always stable in terrestrial settings. To explain this, particularly high excess pore pressures are required at the potential basal shear surface (Talling et al., 2014). For active margins, it is hypothesized that sandy tephra layers are the preferential levels on which translational landslides develop, and this due to their enhanced susceptibility for earthquake-triggered liquefaction compared to the fine-grained (hemi-) pelagic sediments (Harders et al., 2010; Sammartini et al., 2018). However, recent studies on the geotechnical properties of tephra have questioned the propensity of tephra to act as sliding planes (Wiemer and Kopf, 2016).

In terms of triggering mechanisms, human activity (e.g. harbor extensions) plays an important role in generating recent coastal landslides in lakes (e.g., Strupler et al., 2018), fjords (e.g., L´Heureux et al., 2013) and seas (e.g., Dan et al., 2007). For older periods (i.e. before significant human impact), the most commonly assigned trigger for subaqueous landslides is strong earthquake shaking, especially for settings that are close to active fault systems. For lakes, this statement is often supported by accurate temporal correlation between historically documented earthquakes and mapped landslide deposits in their sedimentary infill (e.g., Kremer et al., 2017b; Praet et al., 2017), and by thorough evaluations of alternative non-seismic triggering mechanisms (Moernaut et al., 2007; Brooks, 2016). Accordingly, sequences of intercalated mass-transport deposits (MTDs) in the stratigraphic record have been used to construct long (i.e. Holocene) well-dated paleoseismic records in settings with different levels of seismicity (Karlin et al., 2004; Strasser et al., 2006; Waldmann et al., 2011; Smith et al., 2013; Brooks, 2016 and references therein). The main criterion to confidently assign a seismic trigger is the identification of multiple MTDs on a single stratigraphic level, indicating that several slope failures took place simultaneously (Schnellmann et al., 2002). Glacigenic lakes are often suited for this approach as they typically have deeply-scoured basins with slope segments of variable gradients that can produce individual landslides. Continuous sedimentation leads to the repeated accumulation of slope sequences that can fail when a strong trigger takes place. However, for high seismicity areas and a rather moderate sedimentation rate (~0.1 cm yr^{-1}), it is proposed that lacustrine MTD records can underestimate the frequency of paleo-earthquake recurrence (Moernaut et al., 2009). This is in line with the scarcity of significant landslides during several recent high-magnitude earthquakes along active ocean margins, such as the 2004 M_w 9.1 Sumatra earthquake (Sumner et al., 2013) or the 2010 M_w 8.8 Chile earthquake (Völker et al., 2011), and the long recurrence intervals between MTDs in the stratigraphic record of slope basins (Strozyk et al., 2009; Kremer et al., 2017a). In high-seismicity lacustrine settings, MTDs have been identified in several studies (e.g., Karlin et al., 2004; Moernaut et al., 2007; Praet et al., 2017; Beckers et al., 2018), but were not subjected to a detailed process-based analysis of the linkage between earthquakes and the spatio-temporal evolution of subaqueous slope failures based on the MTD stratigraphic

record. Therefore, it is not yet understood how different preconditioning factors may evolve over time and may affect the potential generation of earthquake-triggered slope failures.

In this study, we develop a detailed MTD stratigraphy for two Chilean lakes (Villarrica and Calafquén) to test and improve the MTD paleoseismic approach for high-seismicity settings with moderate sedimentation rate. By comparison with previous geotechnical studies on slope sequences, we discuss the role of slope gradient and tephra layers on the occurrence and extent of subaqueous slope failure, and how the role of tephra layers can evolve during the depositional history.

2. Setting and previous work

Lake Villarrica and Lake Calafquén are large glacigenic lakes at the western piedmont of the volcanically-active Andes in south-central Chile (Fig. 1). This region has been repeatedly impacted by major and great earthquakes which originated at the subduction megathrust (Cisternas et al., 2005, 2017; Garret et al., 2015; Kempf et al., 2017; Dura et al., 2017; Moernaut et al., 2018 and references therein). The largest "recent" earthquake occurred in AD 1960 (M_w 9.5) and ruptured ~1000 km of the subduction megathrust from 37.5°S to 45°S. The AD 2010 (M_w 8.8) earthquake ruptured the megathrust for ~460 km just north of the AD 1960 rupture. The AD 1960 and AD 2010 earthquakes generated a local (Modified Mercalli) seismic intensity in the study area of about VII½ and VI½-VI¾, respectively (Moernaut et al., 2014). Historical documents covering the last ~500 years describe three other significant megathrust earthquakes near our study area in AD 1575, AD 1737 and AD 1837 (Lomnitz, 1970; Cisternas et al., 2005, 2017). By combining historical data and paleoseismic records, it was suggested that the megathrust earthquake cycle is characterized by a variable rupture mode in terms of rupture location, rupture extent and coseismic slip (Moernaut et al., 2014; Cisternas et al., 2017). Such rupture variability is further supported by geophysical and geodetic data on coseismic and interseismic scales (Moreno et al., 2009, 2018). Well-calibrated turbidite records in lakes Calafquén and Riñihue covering the last 3500-4800 yr revealed that the strongest 1960-like earthquakes (seismic intensity ≥VII½) occur every 292 ±93 yr, whereas earthquakes with an intensity of ≥VI½ take place every 139 ±69 yr (Moernaut et al., 2018).

Lake Villarrica (39°15'S; 72°02'W; 214 m asl) and Lake Calafquén (39°31´S; 72°11´W; 204 m asl) are large (21 x 9 km; 24 x 2-6 km) glacigenic lakes with a maximum depth of 167 m and 212 m, respectively (Fig. 1). The lake basins originated from glacial overdeepening and the build-up of frontal moraines during the last glaciations (Laugenie, 1982). Morphologically, the lakes consist of a deep central basin and a shallower area in their southwestern parts. These southwestern areas comprise several rock basement highs, moraine ridges and isolated sedimentary sub-basins which form our main study areas (Fig. 1)(Moernaut et al., 2017b).

The acoustic basement (i.e. glacial till or bedrock) is overlain by a rather complex and thick sedimentary infill (up to ~120 m thick), of which the largest part is assumed to have been deposited during the early stage of deglaciation. This thick infill is covered by a continuous drape (10-20 m) of hemipelagic sediments, deposited during the Holocene (Moernaut et al., 2017b). In the distal sub-basins, Late Holocene background sedimentation rates of ~0.1-0.2 cm yr^{-1} prevail (Van Daele et al., 2014; Moernaut et al., 2018), which can be considered moderate sedimentation rates for a lacustrine setting. These background sediments consist of diatomaceous mud with a small fraction of organic matter, dispersed volcanic ash particles and minor amounts of terrigenous clays/silts. The background sediments are frequently intercalated with tephra layers, lahar deposits and earthquake-triggered fine-grained turbidites composed of diatomaceous mud (Van Daele et al., 2014, 2015; Moernaut et al., 2014, 2018).

Seismic-stratigraphic analysis documented several voluminous prehistorical landslide deposits (1-6 x 10^6 m^3) in the SW basin of Lake Villarrica (Moernaut et al., 2009), whereas multibeam bathymetric data showed that the AD 1960 earthquake only triggered a few small landslides there (Moernaut et al., 2017a). The presence of other stratigraphic levels containing MTDs has been mentioned in previous studies (Moernaut et al., 2009, 2017a), but no systematic seismic-stratigraphic mapping has been carried out yet. A field of sediment volcanoes and other fluid escape features was identified above a large MTD in Lake Villarrica, and these fluid escape features were interpreted as earthquake-triggered and may thus potentially be used as a paleoseismic proxy (Moernaut et al., 2009).

In Lake Villarrica, a detailed geotechnical study on undisturbed slope sections was carried out by combining detailed bathymetric analyses, in-situ free-fall penetrometer tests (CPTu) and measurements on sediment cores (VILLAR1, 3, 5, 8) including cyclic triaxial tests, direct shear tests and oedometer tests (Wiemer et al., 2015; Moernaut et al., 2017b). These studies documented several areas of focused fluid escape and several units with high excess pore pressure ratios, which are believed to have facilitated the development of large prehistoric landslides on a rather gentle slope (2-4°). The main basal shear surface of these landslides developed just above a fine sandy tephra layer which was deposited ~10.4 kyr ago (Wiemer et al., 2015; Fontijn et al., 2016).

As the main river inflows are located at the eastern extremities of the lakes, the studied isolated sub-basins in the SW are not affected by delta collapses or underflows related to river floods. The composition of the most recent turbidites suggests that these were mostly produced by surficial remobilization of a thin veneer (~5 cm) of hemipelagic slope sediments during earthquakes and did not result from disintegration of subaqueous landslides (Moernaut et al., 2017a). Accordingly, it is assumed that these turbidite records (e.g.

core CAL1 in Calafquén) form a continuous and sensitive archive of past strong earthquakes (Moernaut et al., 2018). Whether the landslide stratigraphy can also be regarded as a reliable natural seismometer in this high-seismicity setting is one of the main subjects of the present study.

3. Methods

3.1 Geophysical data acquisition and mapping of mass-transport deposits

Multibeam bathymetric data were acquired using an R2Sonic 2024 system on Lake Villarrica in January 2013, and a Norbit WMBS system on Lake Calafquén in December 2017. Navigation was recorded by real time kinematic (RTK) corrected GPS with horizontal accuracy in the order of a decimeter (OmniSTAR G2 and Terrastar). Pulse frequency, swath angle and swath direction was adapted on-line in function of water depth and bottom morphology. Data processing (correction for sound velocity, vessel motion, sensor offsets, spike removal) was carried out using CARIS HIPS and SIPS 7.1 (Villarrica) and QINSy software (Calafquén). The presented bathymetric maps have a horizontal grid cell size of 3 m in Villarrica and 2 m in Calafquén.

Reflection seismic surveys using a high-resolution sparker and very-high resolution pinger were executed on Lake Villarrica in December 2001, February 2007 and December 2011, and on Lake Calafquén in February 2007 (SI-Fig. 1). The CENTIPEDE multi-electrode sparker (300 J, main frequency: 400–1500 Hz) was used with a single-channel high-resolution streamer to achieve the full overview of the sedimentary infill of the studied lake basins. For a more detailed analysis of the shallow subsurface, we used the pinger subbottom profiler (main frequency: 3.5 kHz). Navigation and positioning were acquired by standard GPS. All data were recorded digitally and, after bandpass filtering, seismic-stratigraphic interpretation was performed using IHS Markit Kingdom Suite (v. 2015). An acoustic velocity of 1500 m s^{-1} was used for time-to-depth conversions in the water column and the Holocene sediments, which is in agreement with acoustic velocities derived from multi-channel seismic-reflection data on hemipelagic Holocene lake sediments (e.g., Pinson et al., 2013). We use “landslide” and “mass-transport deposit” (MTD) as an overarching terminology for slides, slumps and debris flows, as reflection seismic data alone are not sufficient to establish the exact mass-transport process, and gravitational mass-movements can evolve from one type into another. An original sliding mechanism is supported by the analysis of upslope seismic stratigraphy in Lake Villarrica, which showed that the large MTDs originated from translational sliding along one (or more) distinct basal shear surface(s) parallel to the stratigraphic layering (Moernaut et al., 2017b). MTDs were identified based on their chaotic-to-transparent seismic facies and lens-shaped intercalating geometry forming a positive morphology (following Schnellmann et al., 2002; Moernaut and De Batist, 2011; Praet et al., 2017; Sammartini et al., 2018).

Turbidites (and megaturbidites) are not considered as MTDs as their transport (as turbulent flows) and depositional mechanism are clearly different (e.g., Shanmugam, 2015). Megaturbidites (i.e. turbidites visible on seismic data) can cover the lacustrine basin floor, forming a typical ponding (basin-focused) geometry with a mostly homogeneous, transparent seismic facies (e.g., Van Daele et al., 2015).

We constructed a MTD stratigraphy for isolated distal basins in Lake Villarrica and in Lake Calafquén based on the basic principles of seismic-stratigraphic mapping. The stratigraphic level of each MTD was defined by tracing its top reflection at the distal limits of the MTD. The base of the MTD was not used for this purpose, due to possible erosion in the landslide process. Tracing these horizons throughout the entire basin allowed us to establish a MTD event stratigraphy and reconstruct the relative chronology of different landslides which originated at the basin slopes (e.g., Schnellmann et al. 2002; Waldmann et al.; 2011; Praet et al. 2017; Beckers et al., 2018). If MTDs are assigned to a single horizon, we interpreted a simultaneous occurrence of landslide events within our seismic-stratigraphic resolution, which corresponds to ~100 yr given that vertical seismic resolution is on the order of 10-20 cm and mean sedimentation rates at the studied basins range between 0.1-0.2 cm yr^{-1} (Van Daele et al., 2014; Moernaut et al., 2018). For Villarrica, isopach maps and volume for each MTD were calculated by subtracting the depth of their basal and top horizons and interpolation between seismic lines. In Calafquén, most MTDs are smaller and, therefore, we calculated their volumes by mapping their area and multiplying this by their (visually estimated) average thickness on seismic profiles.

Representative slope gradients for each landslide were measured on the failed section of the slope (i.e. between the headscarp and the base-of-slope). For gentle slopes, the seismic data resolve the slope stratigraphy and we measured the average slope gradient of the basal shear surface. This method is preferable because the inclination of the basal shear surface forms the main controlling parameter governing the downward driving stress for translational slope failure. On steep slopes (>5°), seismic imaging is poor and we measured the average slope of the failed section on the present-day bathymetry. This method is justified because the slope failures are translational in nature, almost fully evacuate the material of the slide scar, and post-failure sedimentation forms a rather uniform drape. Therefore, the present-day slope gradient can be regarded as a good estimate for the inclination of the basal shear surface of a past landslide. Because of the morphological confinement and complexity of our studied lake basins, these strategies differ from the commonly-used method in submarine landslide research, which involves the analysis of adjacent unfailed slope sections (Clare et al., 2018).

The MTD stratigraphy was further complemented by including stratigraphic levels on which sediment volcanoes and/or fluid escape features were found. Their identification follows the procedure outlined in Moernaut et al. (2009): i) Sediment volcanoes consist of intercalating lens-shaped deposits of small dimensions (maximum 2 m high and 80 m wide) and containing low-amplitude chaotic reflections. In map view, they exhibit a rather uniform circular geometry. Their stratigraphic level can be assigned at their pinch-out points. ii) Fluid escape features consist of near-vertical (low amplitude) acoustic wipe-out patches, cross-cutting the otherwise continuous reflections of the background sedimentation (Chapron et al., 2004). Their stratigraphic level is indicated by the base of the undisturbed drape of continuous reflections above them.

3.2 Sediment coring and sedimentological analyses

Hammer-driven piston cores were acquired in May 2009 from an anchored platform in Lake Calafquén (CAL1; Moernaut et al., 2018) and Lake Villarrica (VILL3, VILL4). Moreover, Lake Villarrica was cored for paleoclimate research in December 2007 (VILL1; Heirman, 2011) and for geotechnical research in December 2011 (VILLAR1,3,5,8; Wiemer et al., 2015). Whereas CAL1, VILL3 and VILL4 targeted the basins´ stratigraphy, VILLAR1,3,5,8 and VILL1 were taken on shallower platforms and slopes. On each location, a short gravity core was taken to preserve an intact sediment-water interface. All sediment cores were described macroscopically and logged (0.5 cm steps) with a GEOTEK multi-sensor core logger (MSCL) for gamma density and magnetic susceptibility (MagSus). High-resolution MagSus was obtained with a BARTINGTON MS2E surface sensor. These data allowed the identification of volcanic deposits and the correlation of core segments to construct composite cores (up to 14 m long) on each site (SI-Figs. 2, 3).

Turbidite identification was performed visually as the homogeneous and normally-graded nature of the fine-grained turbidites contrasts with the millimeter-scale laminations of the fine-grained hemipelagic (background) sediments (see e.g., Moernaut et al., 2014). The graded nature is often supported by an upward decrease in MagSus values. For MTD identification, we combined several observations, such as folded and faulted laminations, chaotic and homogenized sections, tephra layers without a stratigraphic equivalent in other cores, and the presence of a turbidite capping a presumed MTD. We labeled the cored turbidites (“Tu”) and MTDs as “resedimentation events” (“Re”) and number them from top to bottom (e.g., Tu: Re5) for each core individually. On core VILLAR8, medical X-ray computed tomography (CT) scans were taken with a Siemens Somatom Definition Flash (Medical University Innsbruck) with a 0.23 x 0.23 x 0.3 mm resolution to evaluate possible soft-sediment deformations near a key tephra layer (“R2”).

3.3 Dating and age-depth models

Radiocarbon ages on piston cores (SI-Table 1) were obtained by accelerator mass spectrometry (AMS) at the Poznan Radiocarbon Laboratory, the National Ocean Sciences Accelerator Mass Spectrometry Facility (NOSAMS) at the Woods Hole Oceanographic Institution and at the Institute of Particle Physics at ETH Zürich. All ages were calibrated using the SHCal13 calibration curve (Hogg et al., 2013). In Villarrica, 20 bulk sediment samples were analyzed, as well as 11 sieved (>125 μm) and hand-picked pieces of terrestrial organic macro-remains. In Calafquén, seven bulk sediment samples were analyzed, as well as seven samples of terrestrial organic macro-remains (see Moernaut et al., 2018).

On the bulk ^{14}C ages in VILL1, VILL3 and VILL4, we applied a soil-related "old-carbon" correction, determined by subtracting the offset (before calibration) between the ^{14}C age of paired samples, i.e. a bulk sample and macro-remains sample at the same stratigraphic level (Moernaut et al., 2017a). We found rather consistent values for this offset value (i.e. 610, 640, 815 yr) and decided to use the average value (688 yr). As paired samples in CAL1 do not give consistent results, the offset value of 512 yr was determined (and applied as a constant) by subtracting the offset between the AD 1575 historic turbidite event and the weighted average of the calibrated ^{14}C age for bulk sediment at the corresponding depth (Moernaut et al., 2018). To allow possible temporal variability of the "old-carbon" offset in all dated cores, we added an error range (1σ) of 100 yr to the offset value. In VILL3, one of the dated macro-remains consists exclusively of aquatic plant material ("macrophyte") as evidenced by a C/N ratio of only 3.8. Accordingly, we applied the same "old-carbon" correction on that sample (VILL3A-IV 35; SI-Table 1). One bulk sample (VILL3A-IV 55.5) was interpreted to be taken in a MTD and was discarded for the VILL3 age-depth model. The gravity cores at the piston coring sites were correlated to other gravity cores in these basins, which were accurately dated by a combination of short-lived radionuclides ($^{210}Pb/^{137}Cs$), varve counting and the recognition of historically-reported volcanic eruptions and their effects (Moernaut et al., 2014; Van Daele et al., 2014, 2015).

The age-depth models for CAL1, VILL1, VILL3 and VILL4 were constructed using the Bayesian software BACON (Blaauw and Christen, 2011), which takes into account the probabilistic nature of calibrated radiocarbon ages. For all age-depth models, event deposits such as turbidites, tephras and lahar deposits were excised and an event-free core depth was used. In VILL3, we inserted a hiatus (~30 cm) in the model at the base of MTD:Re6, as is suggested by tracing the base of the MTD on seismic profiles and by detailed core correlation with VILL4. For CAL1, additional age information from two dated regional tephra layers (Fontijn et al., 2016) was also included in the age-depth model (Moernaut et al., 2018). For VILL3 and VILL4, one marker tephra was included in the age models: i.e. the well-dated "Alpehue Pumice" emitted from Sollipulli Volcano in 2951 ±53 yr BP (Fontijn et al., 2016). This tephra was geochemically fingerprinted in core VILLAR1 and identified in VILL3 and VILL4 by lithostratigraphic core correlation. We integrated the age information

from different dated cores in Lake Villarrica to obtain "final" ages for the seismic stratigraphy, depending on how well the stratigraphic levels are covered by age-depth models (SI-Table 2). For the last 500 yr, we used two turbidites as markers, for which varve counting shows that they were triggered by the historical earthquakes of AD 1960 and AD 1575 (Van Daele et al., 2014). For 500-4000 yr BP, we calculated the average age (and error) of the cored MTDs and turbidites based on the age models from VILL1, VILL3 and VILL4. For 4000-6000 yr BP, we traced the seismic-stratigraphic event horizons towards the overarching age model of VILL1 on the undisturbed platform. As most age-depth models are based on both varve-counted event layers as calibrated radiocarbon dates, we present all derived ages in "yr BP".

4. Results

4.1 Lake Villarrica

4.1.1 Characteristics of MTDs and MTD stratigraphy

The pinger profiles show several voluminous MTDs covering large part of the SW basin of Lake Villarrica (Fig. 2). The largest MTDs (up to 6 m thick; event F on Figs. 2A, 3) have an irregular basal surface, which locally cuts down for 4 m into the underlying stratigraphy. In the deeper parts of the studied basin, the basal reflector of the large MTD-F exhibits very high reflection amplitude and no coherent seismic reflections are visible below (Fig. 2B). Such an acoustic blanking is typical for the presence of free gas in the sediments (e.g., Missiaen et al., 2002) near the lower interface of the MTD. In case of gas blanking, any underlying MTDs were mapped based on i) sparker seismic profiles, which provide a lower resolution but deeper penetration, and ii) interpolation between seismic windows where the lower MTD can be traced. The seismic stratigraphy above the largest MTDs (e.g., MTD-F) is disrupted by fields of sediment volcanoes and focused fluid escape features (Fig. 2A).

Seismic-stratigraphic mapping revealed 11 event horizons, each containing multiple MTDs (Fig. 3; events A-M). The largest landslides of event F originated in the SW and NW edge of the basin by translational failure of a ~6-7 m thick sequence on gentle slope gradients of ~2.5-3°. The main basal shear surface is traceable throughout the basin as a high-amplitude reflection on the pinger data, which corresponds to a fine-grained sandy tephra layer (R2 on Fig. 2)(Wiemer et al., 2015). Upslope, the basal shear surface stratigraphically steps down into older highly-sensitive glacio-lacustrine mud (quick clay). Morphological indications for retrogressive sliding in this area were found, such as an irregular, bottle-neck-shaped headwall trace (Wiemer et al., 2015; Moernaut et al., 2017b). The four largest landslides (> 1 x 10^6 m^3; belonging to events

D, F, I) all initiated on the gentle western slopes of the basin (<4°). Many smaller landslides occurred along steeper basin slopes and their MTDs are restricted to the base-of-slope. There seems to be a large variability in the size of the MTDs, and in the total transported volume associated with each event horizon, ranging from 9.9 x 10^6 m^3 for event F to only 0.04 x 10^6 m^3 for event B (Table 1).

4.1.2 Sediment cores: description, core-to-seismic correlation and dating

Core VILL3 has a composite core length of 12.08 m and covers the last 3.9 kyr (Fig. 4, SI-Fig. 2). It contains two major MTDs (Re6 and Re10) of 2.5 m and 3.3 m in thickness. These deposits are characterized by weakly to strongly folded and faulted laminations and layers, and more chaotic or homogeneous units. The lower part of the Re10 MTD consists of deformed layers of volcanic material such as pumice fragments and medium-grained sandy tephras. Throughout VILL3, nine turbidites were identified ranging from 1 to 10 cm in thickness. Brown or black tephra layers, as well as thinner white-beige clay laminae (distal lahar deposits; Van Daele et al., 2014) are present and are characterized by peaks in density and MagSus. Core-to-seismic correlation for VILL3 was achieved by linking the large MTDs in the core (i.e. Re6-F, Re10-I) with those visible on the seismic profiles (Fig. 4, SI-Fig. 4). Penetration of pinger profiles at this locality is rather limited (~6 m) due to gas blanking, so sparker profiles were used for the lower part of the core. Calculated acoustic velocities for these correlations give reasonable values of 1460 m s^{-1} and 1350 m s^{-1} for the upper and lower part, respectively. The latter value is possibly affected by the presence of free gas in the sediments below MTD-F, lowering the overall seismic velocity and/or affecting the core quality. Core-to-seismic correlation suggests that most turbidites in VILL3 correspond to MTD event horizons on the seismic profiles (see Table 1) (i.e. 1-A, 2-B, 3-C, 4-D, 5-E, 8-G, 9-H). The event-free age-depth model (Fig. 4C) shows a rather uniform sedimentation rate with an average of 0.11 cm yr^{-1}. The hiatus at 5.45 m subsurface (2.49 m event-free depth) determined by core correlation and seismic stratigraphy represents ~150-200 yr of background sedimentation. The well-dated tephra at 6.5 m subsurface (3.33 m event-free depth) related to the Alpehue eruption is located in line with the age-depth model (Fig. 4C), which suggests a good reliability. However, two of the dates based on macro-remains fall aside the age-depth model, leading to a relatively large modelled error (±250 yr) at the depth interval 2-3 m.

Core VILL4 has a composite core length of 8.83 m and covers the last 3.1 kyr (Fig. 5, SI-Fig. 3). It was taken at the base-of-slope in a stack of small-scale MTDs observed on the seismic profiles. VILL4 contains eight MTDs ranging in thickness from 15 cm to 75 cm, and 10 turbidites with thicknesses of 2 to 7 cm. Two MTDs (Re5 and Re13) exhibit a nearly-intact stratigraphic sequence that either corresponds to the sequence below ("doubled stratigraphy" at Re5) or is fully allochthonous (Re13), as was determined by detailed core

correlation with VILL3. All other MTDs show folded/faulted units and are directly covered by a turbidite. As in VILL3, lahar deposits (up to 12 cm thick) form an important part of the cored sequence, which can be explained by the vicinity of both sites to one of the main lahar inflow points on the south shore of Lake Villarrica (Van Daele et al., 2014). Core-to-seismic correlation for VILL4 was established through one-by-one correlation of the eight MTDs in the core with mapped MTDs on the seismic profiles crossing the core site (Fig. 5). This correlation leads to a realistic calculated acoustic velocity of 1490 m s^{-1}. From the cored MTDs at VILL4, all but one corresponds to a seismic horizon of multiple MTDs (i.e. 1-A, 3-B, 5-D, 9-F, 13-G, 15-H, 18-I). The event-free age-depth model (Fig. 5B) shows a sedimentation rate (~0.16 cm yr^{-1}), which gradually decreases over time. The Alpehue tephra deposit at 6.43 m subsurface (4.33 m event-free depth) is ~300 yr older than its age derived from the age-depth model, indicating a rather poor quality for the lower part (2000-3000 yr BP) of our model. Therefore, we did not make any direct chronostratigraphic correlations between the event records of VILL3 and VILL4.

Core VILL1 (location on Fig. 6A) has a composite core length of 13.75 m and covers the last 9.4 kyr (Fig. 6B, C). It was taken at 82 m depth on a platform in the northern part of our study basin (Fig. 2). VILL1 was analyzed with a wide range of proxies for paleoclimate research purposes (Heirman, 2011). The sediments consist of finely laminated diatomaceous mud, and 62 black, sandy tephra layers. In this core, an important volcanic unit was observed at a depth of 5.6-6.2 m and is composed of two tephra layers (5.63-5.72 m: coarse sand; 6.03-6.18 m: medium sand) separated by fine silty clastic sediments. VILL1 also contains 72 beige-colored, fine silt laminae, which were produced by interflows generated by lahars entering the lake (Van Daele et al., 2014). The central platform is devoid of MTDs or erosional unconformities, so this core can be regarded as a continuous sediment sequence, allowing dating the overall seismic stratigraphy (Fig. 6). Core-to-seismic correlation was facilitated by linking high-amplitude reflections with peaks in γ-density (e.g., R1 on Fig 6B) and leads to a calculated acoustic velocity of 1440 m s^{-1}. The age-depth model (Fig. 6C) shows some sharp changes in the sedimentation rate in the upper 2 m (event-free depth) of the core, for which we did not encounter any evidence in the form of changing laminae thickness, sediment composition or seismic facies. Therefore, we speculate that these apparent changes in modeled sedimentation rate relate to a changing magnitude of the “old-carbon” effect over time. Accordingly, the dates for the seismic stratigraphy around ~1 m depth at this site may be significantly too old (order of a few 100 yr), producing the sharp knickpoints in the curve.

Core VILLAR1 has a composite length of ~8 m and covers the last ~13 kyr (Fig. 6D, E). It was taken on a shallow-water platform at 22 m depth, in between the headscarps of large subaqueous landslides and a large composite pockmark. VILLAR1 was analyzed for geotechnical purposes (Wiemer et al., 2015; Moernaut

et al., 2017b) and contains a high-quality record of regional tephra layers (Fontijn et al., 2016). No distinct lahar deposits were found as its elevated position is out of reach of lahar-induced interflows along the lake thermocline. The lower 70 cm of the core consists of clastic fine-grained silts and clays and relates to a glacio-lacustrine environment that persisted from ~17.5 kyr to 12.8 kyr. For the present study, the main feature is the presence of a 3 cm thick fine-grained sandy tephra layer ("R2"), which just underlies the main basal shear surface of event F. Core-to-seismic correlation was achieved by linking high-amplitude reflections with peaks in γ-density ("R1" and "R2"), and leads to a realistic calculated acoustic velocity of 1460 m s^{-1}. The R2 reflection in core VILL1 was identified by transferring the seismic stratigraphy from VILL1 to VILLAR1 and matching the sequences of seismic facies (Fig. 6D).

4.2 Lake Calafquén

4.2.1 Characteristics of slope failures and MTD stratigraphy

The pinger seismic profiles show numerous stacked MTDs at the foot of the basin slopes (Fig. 7A) and one outstanding thick event covering the entire basin (event-M; max. 12 m thick). Large-scale sediment escape features are only observed above the large MTD-M. The basal horizon of event M cuts down to maximum 6 m into the seismic stratigraphy at the foot of slopes. The undisturbed uppermost seismic units (upper 5 m) show a gentle basin-focused geometry.

The established MTD event stratigraphy for Lake Calafquén (Fig. 8) contains 14 events of multiple landslides. The MTDs related to events M, C and A can still be traced on the present-day lake bottom as lobe-shaped positive morphologies. MTD-M is an outstanding voluminous event (6.2 x 10^6 m^3), for which the main MTD is formed by at least three different slope failures, which originated in the SW, N and SE of the basin. These slope failures were identified based on the position of frontal ramps in the basin and on headwall scarps visible on the seismic profiles and the multibeam bathymetric map (Fig. 8). Event M also includes the formation of a long, narrow and deep gully (approx. 2200 x 200 x 11 m) in the basin plain, connecting the deepest basin of Lake Calafquén in the north (215 m depth) with the slope failure area in the southeast (Fig. 8). The stratigraphic level of this gully locally steps up towards the east and is covered by highly-irregular MTDs (Fig. 7B, C), indicative of scarp adjustments soon after gully formation. The gully originated shortly after the deposition of the main MTD-M, as constrained by i) the similar seismic units on top of the MTD-M and the gully infill, and ii) the fact that the gully cross-cuts the main MTD-M (Fig. 7B, C). The similar overlying stratigraphy also indicates that there are no large-scale mass-transport processes active in the gully since its formation. The development of event M can thus be summarized in three steps which happened in close

succession: i) slope failure along the SW, N and upper SE slopes of the basin, leading to a thick MTD-M covering the entire basin, ii) slope failure on the gentle lower SE slopes including gully formation in the basin and MTD deposition in the deepest (non-mapped part of the lake), iii) local adjustments of headscarps and gully side-walls.

For the SE slope failure area, the basal shear surface of MTD-M developed just above a continuous strong reflection in the stratigraphy (Fig. 7D), which forms the stratigraphic equivalent of the R2 horizon in Lake Villarrica. This identification is based on seismic-stratigraphic correlation between the VILL1 seismic stratigraphy and the stratigraphy upslope of the SE headscarp in Calafquén (inset in Fig. 7D). Such inter-lake correlation is justified by the observation that strong reflections in the Chilean lakes often correspond to regional tephra layers deposited in multiple neighboring lakes (Fontijn et al., 2016). At present, the basal shear surface of MTD-M is buried by approx. 5.5 m of post-failure sediments in the south eastern sub-basin. This post-failure sequence exhibits a discrete zone of vertical acoustic wipe-out (5 m high) rooted in the former basal shear surface (of MTD-M) and reaching up to the present day lake bottom (Fig. 7D). This wipe-out zone involves a vertical reflector offset by ~0.8 m, in which the downslope part of the sequence forms the downthrown side of this synsedimentary fault. We interpret this feature as an indicator of the development of incipient gravitational sliding: i.e. suggesting that this 5.5 m thick sequence may fail as a translational slide in the future. Some smaller irregularities in the reflection continuity were found in the sediments just overlying the former basal shear surface (R2). This unit is ~0.5 m thick and shows short wipe-out patches and minor reflector offsets and is interpreted as a unit of mainly in-situ deformed sediments, with possibly minor slumping (see section 4.5 and 5.3).

4.2.2 Sediment core: description, core-to-seismic correlation and dating

Core CAL1 has a composite length of 8.6 m and covers the last 3.5 kyr (Fig. 9)(Moernaut et al., 2018). It was taken in the central part of the study basin where a continuous sequence overlying the large MTD-M is observed on the pinger profiles (Fig. 7A). CAL1 contains diatomaceous mud, two (dated) regional tephra markers and 13 turbidites, the lowermost of which directly overlies the MTD-M. Several coarse and thick (~5 cm) lahar deposits are present due to the vicinity of the lahar inflow paths of Villarrica Volcano (Fig. 1)(Van Daele et al., 2014). Core-to-seismic correlation for CAL1 was achieved by linking abrupt changes in the density profile with strong reflections and by the identification of the large MTD-M (Moernaut et al., 2018). This correlation suggests an acoustic velocity of 1300 m s^{-1}. This low value can possibly be explained by deformation during the piston coring process and gas expansion during core retrieval. From the cored turbidites at CAL1, nine turbidites correspond to a seismic horizon of multiple landslides and fluid escape

features (i.e. 1-A, 2-B, 3-C, 4-D, 5-E, 7-G, 8-H, 10,-J, 13-M; Fig. 9), whereas the other four turbidites only link to a level of fluid escape (6-F, 9-I, 11-K, 12-L). The age-depth model shows rather constant sedimentation rate of 0.11 cm yr^{-1} and its good quality is confirmed by a regional tephra marker (Moernaut et al., 2018).

4.3 Overall event stratigraphy of Lake Villarrica and Lake Calafquén

The detailed correlation of the event stratigraphy on seismic profiles (i.e. MTDs, fluid escape structures) with the sediment cores (MTDs, turbidites) allows the establishment of a compound event stratigraphy of each study basin (Table 1). The main framework is formed by the stratigraphic levels of multiple MTDs, most of which correspond to fluid escape horizons (Villarrica: 15 out of 16; Calafquén: 9 out of 9) when only considering the stratigraphic depths with excellent seismic data quality. Lower sections have a more diffuse low-amplitude seismic signature, hampering the analysis of fluid escape features. In Villarrica, two fluid escape levels (C and E) were not associated with multiple landsliding (see also Moernaut et al., 2009), but potentially do correlate with turbidites in the sediment cores. Two turbidites in VILL3 and nine turbidites in VILL4 cannot be associated with a seismic-stratigraphic event level. All cored turbidites and MTDs in VILL3 have a counterpart in VILL4 as turbidite or MTD. In Calafquén, four fluid escape events do not relate to the MTD stratigraphy, but do correlate with turbidites in CAL1. All other turbidites in CAL1 correspond to events of multiple landsliding.

4.4 MTD volume and slope gradient of failure

In order to examine the potential role of slope gradient on landslides volume, we compared the average slope gradient of the failed slope section for each mapped MTD with the calculated MTD volume (Fig. 10). Most landslides took place on slopes of 7-13°, whereas the four largest landslides occurred on slopes less than 4°. Despite significant data scatter, we interpret a (power law) trend of decreasing landslide volume with increasing slope gradient. Remarkably, the three largest landslides in each lake make up ~75% of the total displaced sediment volume of all mapped landslides in each lake (Villarrica: 41 landslides; Calafquén: 55 landslides). Therefore, these infrequent large landslides can be regarded as the main drivers for gravitational sediment transport in the studied basins over the last 10 kyr.

4.5 Position of tephra layers, soft-sediment deformations and basal shear surface

Besides the identification of MTDs and associated landslide scarps (Moernaut et al., 2017b), the seismic profiles also exhibit thin (~0.5 m) units of in-situ deformed sediments. These units consist of chaotic and

disrupted reflections and/or intact blocks separated by small vertical offsets (Fig. 11A). The in-situ deformed units do not intercalate in the stratigraphy (like MTDs) and the sediments above the basal shear surface were not evacuated. They occur over large (near-) horizontal areas and are more pronounced where slopes are a bit steeper (up to ~2°). These units overly high-amplitude continuous reflections, associated with the presence of sandy tephra layers of a few cm thickness (R1 in VILL1; R2 in VILLAR1) (Fig. 11B, C). The thin deformed unit (~0.5 m) above R1 (Fig. 11A) is at the stratigraphic level of multiple MTD event J, so we interpret that these were formed simultaneously. A thicker in-situ deformed unit (~3.2 m) was identified in the same area, but on steeper slopes (1.5-2°), and is associated with MTD-F, the largest MTD event in Lake Villarrica.

In sediment core VILL1 (5.05-5.63 m), the event J in-situ deformation (Fig. 11B) consists of folded and chaotic sediments that directly overlie a sandy tephra. Below the tephra and above the deformed unit, the lacustrine sediments exhibit horizontal laminations indicating an undisturbed position. Remarkably, the upper ~15 cm of the deformed unit consist of the same tephra material as the basal tephra R1. Similar observations on in-situ deformations were made at an outcrop (37.5°S; 71.27°W) south of Lago Laja by Melnick et al. (2006). At the outcrop, laminated glacio-lacustrine deposits were plastically deformed, showing convolute layering above a basal sandy tephra. This basal tephra also intruded into the deformations and covered the entire deformed unit. The over- and underlying units are horizontally laminated and undeformed.

The largest landslide during event F took place in the SW extremity of Lake Villarrica (Fig. 3). Its main basal shear surface developed a few cm above the R2 tephra (Fig. 11C), which has been cored at the unfailed platform (VILLAR1) and in the failed area (VILLAR3,5,8). CT scans of VILLAR8, located near the edge of the unfailed platform, show thin in-situ deformations above the R2 tephra (Fig. 11C, D). On the failed slope, the basal shear surface is overlain by ~30 cm of chaotic MTD debris (Fig. 11C, E), deposited just after the 6-7 m thick slope sequence slid downwards.

5. Discussion

5.1 Challenges for MTD stratigraphy

The construction of a MTD stratigraphy based on 2D subbottom profiler data is subjected to several limiting factors inherent to the type of data, the nature of landslides and MTDs, and the decisions taken by the operator. These factors all affect the quality of the MTD stratigraphy and the derived paleoseismic records,

but can be partially addressed by new method improvements (listed in Table 2). Data type limitations relate to the vertical resolution (typically dm-scale) and the survey grid density (typically a few hundred m), which may cause a failed detection of very thin and/or spatially limited MTDs. Consequently, the MTD paleoseismic record may lack those earthquakes which only left a limited sedimentary imprint on the lake bottom. Moreover, data density can strongly affect MTD volume calculations (Clare et al., 2018). Possible improvements involve a densification of the survey grid at the foot of slopes, and post-processing of high-quality seismic data acquired by innovative 3D subbottom profiler techniques (e.g., Vardy et al., 2017). Another methodological factor is the low signal-to-noise ratio in deeper parts of the sedimentary infill due to the gradual decrease of transmitted (and reflected) seismic energy with depth. In cases of gas-charged sediments, strong impedance contrasts may reflect most seismic energy and gas blanking occurs below the gas-rich horizon. These depth-related factors result in apparently lower amounts of MTDs in older parts of the stratigraphic sequence and it is therefore crucial that this effect is taken into account when comparing the recurrence and size of multiple MTD events. One could apply lower-frequency seismic sources (e.g. sparker, airgun) to better visualize the older strata, but due to their lower vertical resolution, this will not solve the problem of thin MTD detection.

The nature of landslides and MTDs also produces limitations for MTD stratigraphy. Repeated landsliding can lead to stacked MTDs which are indiscernible, especially when significant basal erosion occurs. Large buried MTDs often exhibit abundant fluid escape features in the overlying units (Moernaut et al., 2009), which does not permit a precise identification of the MTD top horizon. In such situations, one should analyze the most distal or lateral parts of MTDs which are typically non-erosive and bear fewer fluid escape features. Moreover, the obtained MTD stratigraphy can be evaluated by correlation with turbidite records in more distal cores.

The last factor, which is often neglected, is the operator subjectivity in the assignment of stratigraphic levels and grouping of MTDs by tracing horizons throughout a basin or across basins. “Wishful thinking” may often lead to the grouping of MTDs on a single level, whereas in reality they may relate to closely-spaced levels. Such bias is difficult to account for, but may be reduced by comparing results of multiple operators and/or by a standardized protocol including decision trees for commonly-encountered challenges, like the examples listed above.

5.2 Preconditioning factor: slope angle

The driver for all translational subaqueous landslides is the downslope component of gravitational overburden stress imposed on an inclined potential basal shear surface. In terms of preconditioning, the timing of landslides is thus influenced by sedimentation rate (charging the slope with sediments) and the time since a previous failure event occurred on that slope segment (Strasser et al., 2011). Moreover, slope gradient defines the downslope component of the overburden stress, and slope morphology can determine the length of the failing slope segment (Moernaut and De Batist, 2011; Puzrin et al., 2015), assuming the simplest case in which no spatial changes in mechanical stratigraphy occur. A catalogue of submarine landslides in the North Atlantic (including fjords) led to the suggestion that the largest landslides mainly take place on the gentlest slopes (<2°) (Hühnerbach et al., 2004). Our case study of two well-constrained lacustrine basins reinforces this suggestion as the four largest landslides (3.6-6.3 x $10^6 m^3$) of both lakes occurred on the gentlest slopes in the database (<4°). The difference in volume between these four events and the rest of the lake records is striking, given that ~75% of the total transported volume in each lake occurred during these large events (Fig. 10). By comparison with tsunamigenic sublacustrine landslides in glacigenic peri-alpine lakes (Hilbe et al., 2015; Strupler et al., 2018), we can expect these large events to have caused lake tsunamis with runup heights in the order of ~1-5 m, whereas the smaller landslides likely did not produce significant waves. Our study only addresses landslides on "lateral slopes" (sensu Sammartini et al., 2018) with hemipelagic sedimentation, a setting where landslides are typically of translational nature. For such slopes, our MTD dataset highlights that "worst-case" tsunami hazard assessments should especially focus on gentle slopes, where landslides typically occur infrequently but involve the largest volumes.

It is remarkable that such gentle slopes can fail after all, as their slope gradient is well below the typical friction angles for different sediment types. Therefore, to allow static slope failure, the effective stress near the potential basal shear surface needs to be reduced by high excess pore pressure reaching 80-95% of the lithostatic stress for a 2° slope, and 60-90% for a 4° slope (Urlaub et al., 2015). In Lake Villarrica, these conditions are met, as in-situ dissipation tests near landslide scarps document high excess pore pressure ratios of 70-90% (Moernaut et al., 2017b). At the unfailed platform (VILLAR1), excess pore pressure ratios of only 30-40% exist, possibly explaining why this slope segment remained stable. These elevated pore pressures in Lake Villarrica are hypothesized to arise from repeated focused fluid transfer from deeper glacier-proximal units in the stratigraphy (Moernaut et al., 2017b).

5.3 Preconditioning factor: tephra

Sandy tephra layers have been proposed to act as sliding planes for translational submarine landslides at active margins, due to their potential to liquefy under earthquake loading (Harders et al., 2010). Indeed,

liquefaction can occur in well-sorted loosely-deposited granular sediments under undrained conditions, when earthquake-induced excess pore water pressure reduces the effective confining stress to nearly zero, causing a drastic loss of shear strength. This phenomenon is thus especially relevant for sandy tephra layers which are shallowly buried under fine-grained lake sediments, because there is little confinement, a low-permeability barrier, and a very loose packing of the tephra due to the typical quiet water conditions in lakes (Fig. 12A). Under such shallow burial, seismic shaking induces alternating extensional and compressional stress, leading to fast pore pressure rise because the cohesionless character of clean sand makes it very susceptible to extensional shearing (Mohamad and Dobry, 1986). Consequently, sandy tephra layers can be regarded as especially "weak" units under dynamic loading conditions, when compared to typical fine-grained hemipelagic sediment. This process can explain the in-situ deformed units located above tephra layers, which we observed in core VILL1 and in an outcrop (Fig. 11A, B). In both cases, the tephra was buried approximately 0.3-0.5 m below the lake bottom at the time of shaking. The overlying silt-sized lacustrine sediments deformed plastically, but the lack of a significant slope gradient prevented it from gravitational sliding. Seismically-induced collapse of the loose tephra package led to fast pore pressure rise and liquefaction. Upwards escaping pore fluids from the lower part of the tephra generated fluidization of its upper part, which then got entrained into the deforming lacustrine sediments.

With ongoing burial of a tephra layer, confinement increases and grain packing becomes denser, making earthquake-triggered liquefaction more and more improbable (Garga and McKay, 1983; Obermeier, 1996). Also, with larger confinement, the cyclic loading will involve little to no extensional stress on the cohesionless tephra, which will present a higher cyclic strength than in isotropic (near-surface) conditions (Mohamad and Dobry, 1986). Repeated shaking of tephra layers −without liquefying them− may additionally lead to a denser packing, through the process of "seismic strengthening" (Fig. 12A). This involves the coseismic build-up of excess pore pressure and subsequent dissipation during interseismic times, typically leading to (apparently) overconsolidated and strengthened sedimentary sequences in high-seismicity settings (Locat and Lee, 2002; Sawyer and DeVore, 2015; ten Brink et al., 2016). Overall, the declining liquefaction susceptibility with age and depth strongly contrasts with the hypothesis that liquefaction of tephra layers forms a major controlling factor for large submarine landslides on active margins. Wiemer et al. (2015) tested the dynamic response of different Lake Villarrica sediments, by simulating buried conditions (~20 m) using strongly anisotropic initial stress conditions for the undrained cyclic triaxial tests. They revealed that the tephra layer R2 yields the highest cyclic shear strength in the sequence compared to the hemipelagic diatomaceous mud and glacio-lacustrine clay, and is thus the least likely to develop into a basal shear surface during earthquake shaking. Nevertheless, the R2 tephra may have played a role in the development of translational sliding, because, due its high permeability, coseismically-generated excess pore

pressures in this tephra may have migrated instantly to the interface with the lower-permeability hemipelagic sediments above. There, it repeatedly caused a local reduction in effective stress, stiffness and strength, resulting in larger deformations and the initiation of translational sliding when all conditions are met (Wiemer et al., 2015).

Following the above argumentations, we developed a simplified sequential model of how tephra layers can affect the stability of a an accumulating slope sedimentary sequence, using the combined stratigraphy at VILL1 and VILLAR1 as reference (Fig. 12B): i) the R2 tephra (~3 cm thick; ~10.4 kyr BP) is deposited and buried under ~4 cm of hemipelagic sediments; ii) the first strong earthquake induces liquefaction of R2 and in-situ deformation of its overlying sediments; iii) ~6.4 kyr of background sedimentation takes place. Repeated earthquake shaking (21 times given a 300 yr recurrence interval; Moernaut et al., 2018) may have densified the R2 tephra and further weakened the directly overlying sediments by transfer of excess pore fluids; iv) the R1 tephra (~8 cm thick, ~4 kyr BP) is deposited and buried under ~40 cm of rapidly-deposited post-eruption clastic sediments (in VILL1); v) the first strong earthquake induces liquefaction of R1 and large-scale in-situ deformation of the overlying sediments (event J, ~3.9 kyr BP); vi) ~0.5 kyr of background sedimentation takes place until a strong earthquake triggers large-scale translational sliding above R2 (event I, ~3.4 kyr BP).

5.4 Landslide cycle and preconditioning

By mapping the spatio-temporal history of MTDs in both lakes (Figs. 3, 8), and grouping them into events of multiple MTDs, we were able to examine the evolution of transported volume by landslides over time (Fig. 13). In the oldest parts of the records (~7.4-4.0 kyr BP), several events with minor (<0.1 x 10^6 m^3; both lakes) to moderate volume (0.1-1.2 x 10^6; Calafquén) took place on relatively steep slopes (7-20°). The middle part (4.0-2.0 kyr BP) includes three large events (>1.2 x 10^6 m^3) and two small events in Lake Villarrica, and one large and one small event in Calafquén. The large events occurred on gentle slopes of <4° (see section 5.2). The youngest part of the record consists of numerous small and moderate events, mostly occurring on slopes of ~7-20°. The large events all used tephra R2 as main basal shear surface, which was deposited around 10.4 kyr BP. Since then, ~6.6-8.4 kyr passed before large translational sliding took place on different slope segments with a gentle gradient. This period allowed 5.5-6.8 m of slope sediment to be deposited on the R2 tephra, which seemed to have provided the critical amount of overburden stress to facilitate gravitational failure during earthquake shaking. Since the last large event in Calafquén at 3.5 kyr BP (event M), ~5.5 m of slope sediment accumulated on R2 (Fig. 7D), which is close to the thickness of the failed slope during event M (~6 m). Accordingly, indicators for incipient failure (see section 4.2.1) suggest that failure of

this 1-1.5° dipping sequence may take place once the overburden stress has reached the threshold for failure when combined with strong seismic shaking. This would mean that the upper interface of R2 can repeatedly act as basal shear surface for translational slope failures separated by several thousands of years. We can thus regard this repeated sliding as landslide "cycles", which start with the gradual burial of the tephra layer and end with the large landslide event(s) (Fig. 13). The first strong earthquake in the earliest phase of the cycle typically induces plastic in-situ deformations above the tephra (Fig. 12B). For such gentle slopes, much more time is needed to achieve near-critical stability conditions than for steeper slopes (e.g., Strasser et al., 2011).

Some of the largest MTD events involved the simultaneous triggering of multiple large landslides (e.g. event F in Villarrica, event M in Calafquén), suggesting that either i) the evolution of slope preconditioning is equal at different slopes in different parts of the lake, or that ii) these events relate to exceptionally strong shaking, initiating failure of slopes which were not fully preconditioned yet. It may seem rather unlikely that local slope stability reached similar conditions at the same moment, due to spatial variability in sedimentation rate and slope gradient, and therefore, one may favor the hypothesis of exceptionally strong shaking. However, slope preconditioning is not per se a gradual process, but can be provoked by sudden geological and sedimentary events. For example, voluminous sliding (>3 x 10^6 m^3) in both lakes only initiates shortly after the deposition of tephra R1, which corresponds to the ~4.0 kyr BP Pucón volcanic event (VEI=5) (Fontijn et al., 2016), the strongest eruptive episode of Villarrica Volcano during the Holocene. This volcanic event started with a Plinian explosive outburst (Moreno and Toloza, 2015) and culminated in a series of extensive pyroclastic flows on all flanks of the volcano and the formation of a 2.2 km wide caldera (Silva Parejas et al., 2010). We hypothesize that this Pucón volcanic event may have additionally preconditioned the slopes towards failure, and this in a two-fold manner:

- Eruption-related seismic shaking: the successive volcanic events may have been associated with repeated and prolonged seismic shaking around the volcano, potentially increasing pore pressure in susceptible stratigraphic layers. Moreover, caldera collapses are known to generate the strongest volcano-related earthquakes (Zobin, 2001) with maximum documented earthquake magnitude and intensity of 7.0 and VI-VII, respectively.

- Sudden overburden loading: at our study sites, the related deposits of air-fall and post-eruption material have a thickness ranging from ~0.2 m (VILLAR1) to ~0.7 m (VILL1) and an average bulk density of 1.8 g cm^{-3}. Assuming the end-member scenario in which this sudden overburden weight is fully transferred into pore pressure increase at the potential basal shear surface, we calculate an increase of overpressure ratio of ~13-

18% for this event. This value can be regarded as a maximum value as our end-member scenario assumes instantaneous loading and an impermeable cap above the potential basal shear surface.

Given these potential mechanisms for elevating pore pressure during the Pucón eruption cycle, it seems possible that the slopes experienced a punctual decrease in overall stability, which can explain why large landsliding started shortly after ~4.0 kyr BP. We do not constrain how fast excess pore pressure may have dissipated after this volcanic event and whether these migrating fluids may have locally accumulated and favored slope failure a significant time (100s of years) after the volcanic event. In any case, such hypotheses remain difficult to test without detailed investigations of each involved slope segment by a combined geotechnical, numerical, morphological and seismic-stratigraphic approach.

5.5 Paleoseismic events and implications for landslide paleoseismology

Synchronicity of lacustrine slope failures is assumed when several MTDs share the same seismic-stratigraphic horizon. Such synchronicity suggests a regional trigger mechanism, such as strong earthquake shaking (Schnellmann et al., 2002), especially when other trigger mechanisms are highly improbable. This paleoseismic method exclusively builds upon the mapping of multiple coeval MTDs, as a single lacustrine slope failure can be caused by a wide range of triggering mechanisms, such as rapid slope loading and oversteepening at an active delta front, wave action during storms, lake-level drops leading to sudden gas discharge, etc. (Girardclos et al., 2007). All our mapped MTD levels fulfill the synchronicity criterion within the vertical resolution of our seismic stratigraphy (section 5.1), and can thus be regarded as paleoseismic events. As the studied basins are close to each other (28 km) and the main earthquake triggers relate to large megathrust ruptures (>100 km long) at the subduction interface (Moernaut et al., 2014), we assume that most recorded paleo-earthquakes in one lake must also have produced MTDs in the other lake. So, to evaluate the potential and limitations of the MTD paleoseismic approach, we attempted to cross-correlate events between both records (Fig. 14). We further complement these records by including the stratigraphic levels with fluid escape features and cored turbidites, which are both considered as paleoseismic proxies in this specific lake setting (Moernaut et al., 2009,2018). The period 7.5-4.0 kyr BP was omitted from this correlation due to poor age-control in Calafquén (extrapolation of age-depth model) and poor seismic data quality (acoustic blanking) in Villarrica.

The historical earthquake events in AD 1575 and AD 1960 are recorded in both lakes, where the corresponding MTDs and turbidites are accurately dated by varve-counting and short-lived radionuclides (Moernaut et al., 2014). For the prehistorical periods, the relatively large error bars of the age-depth models

(±200 yr), provide a large degree of uncertainty for correlation assessments. Ten potential correlations were proposed (Fig. 14). The only large event in Calafquén (M) potentially correlates with the 2nd largest event in Villarrica (I). Its large impact on the sedimentary infill of Calafquén possibly obliterates any evidence for smaller MTDs that may have occurred in a few centuries before event M. This potentially can explain the absence of mapped MTDs in Calafquén in the interval ~4-3.7 kyr BP, during which Villarrica experienced a large event (event J). Alternatively, it may be possible that part of the first stage of the multi-stage event M in Calafquén (see section 4.2.1) occurred in the ~4-3.7 kyr BP interval and forms the counterpart of event J in Villarrica. The other two voluminous MTD events in Villarrica seem to have a small counterpart in Calafquén (F-H; D-F). For 0.5-1.0 kyr BP, two MTD events in Calafquén were found, but no MTD events in Villarrica. From this preliminary correlation attempt, we conclude that we cannot really assess the multi-lake impact of individual prehistoric earthquakes, due to the relatively short interval between paleoseismic events recorded in the seismic stratigraphy (Villarrica: 434 ±192 yr; Calafquén: 292 ±93 yr) and the comparably large uncertainties of the age-depth models (~200 yr). Additional dating uncertainty is introduced by i) a possible time-variably old-carbon effect for the bulk samples, and ii) the grouping of small organic macro-remains which can have different histories of how and when the material was transported and buried in the lake sediments. Moreover, uncertainty also affects the core-to-seismic correlation and the tracing of seismic horizons in areas of complex stratigraphy.

Given these limitations in event-per-event correlation, we alternatively assess our paleoseismic approach by comparing average recurrence rates and their variability between sites and record type. Moernaut et al. (2018) calculated the average recurrence interval (arithmetic mean) for turbidites in CAL1 to be 292 ±93 yr (1σ of the distribution of recurrence intervals), and suggested that this represents the recurrence interval of M_w ≥8.6 megathrust earthquakes in the region (see also Cisternas et al., 2005). As seismic data quality is poor below the CAL1 core and due to the occurrence of four turbidite levels that lack a multiple MTD event, the average recurrence interval exclusively based on MTD stratigraphy is much longer: 561 ±312 yr. However, if we consider also fluid escape features and limit our analysis to the last (cored) 4 kyr, we see that all cored turbidites are represented in the seismic event stratigraphy.

For Lake Villarrica, the average recurrence interval of the seismically-resolved MTD stratigraphy is comparable: 600 ±238 yr. This value decreases to 434 ±192 yr when limiting the analysis to the acoustically well-resolved section (i.e. the last ~4 kyr) and including the levels of fluid escape and VILL3 turbidites. Yet, this value is value is still higher than the reference value of 292 ±93 yr for the recurrence of the largest earthquakes in the region, and it seems that the Villarrica paleoseismic record (based on VILL3 and seismic stratigraphy) forms an underrepresentation of large earthquakes. This is especially clear for the 0.5-1.0 kyr

BP gap in the VILL3 paleoseismic record (Fig. 14), which cannot be explained by operator bias or dating uncertainties. Interestingly, for core VILL4, the combined record of MTDs and turbidites provide a much shorter average recurrence interval of 179 ±111 yr. When neglecting the anomalous absence of events between 600 and 1100 yr BP, the VILL4 record leads to a recurrence interval as short as 157 ±63 yr. This is much shorter than the 292 ±93 yr for Mw ≥ 8.6, but is near the average recurrence interval (138 ±69 yr) for M_w 7.7-8.5 earthquakes, as determined from turbidite records in Lake Riñihue, located 60 km to the south of Villarrica (Moernaut et al., 2018). It thus seems that the most complete and sensitive paleoseismic record in Villarrica is present at VILL4, a base-of-slope site that contains both small MTDs and turbidites which originated on a 10-15° dipping slope (Fig. 5).

As individual slope segments need a certain time to recharge with sediments after slope failure took place, there may be a crucial ratio of sedimentation rate vs. earthquake recurrence interval for making the MTD paleoseismic method work. Because of this, the most consistent results have been achieved in low-to-moderate seismicity settings, such as the Swiss Alps (compiled in Kremer et al., 2017b), Lake Tahoe basin in the USA (Smith et al., 2013) or Southern Patagonia (Waldmann et al., 2011). In high-seismicity settings, distal proglacial lakes may offer the required high sedimentation rate in the order of 0.5-1.5 cm yr^{-1} (of fine-grained sediments) to overcome this slope recharging issue, but paleoseismic studies in proglacial lakes are largely absent (Praet et al., 2017).

Despite possible underrepresentation of large earthquakes, well-dated MTD records may help to strengthen paleoseismic records derived on other lakes, or on other types of archives (e.g., tsunami deposits, subsidence) by adding that there was “strong seismic shaking” during the event. Comparison with historical earthquakes (Moernaut et al., 2014; Van Daele et al., 2015) and slope stability modeling (Wiemer et al., 2015) shows that multiple MTD formation in the studied lakes requires a local seismic intensity of ≥VII½, which is somewhat higher than the intensity threshold of VI-VII derived from Swiss lakes (Kremer et al., 2017b). Taking the subduction megathrust as dominant source of seismicity in our study area, this means that multiple MTD events exclusively represent the events with the largest seismic shaking in this region (e.g., M_w 9 type earthquakes) and neglect the more frequent “smaller” earthquakes (e.g., M_w 7-8 type earthquakes). The latter can potentially be investigated by looking into turbidite records that are generated through remobilization of a thin veneer of surficial slope sediments (Moernaut et al., 2017a, 2018). The main challenge for such turbidite records is to select a core site that is close enough to the slope sediment source area, but far enough from voluminous MTDs that strongly reshape bottom morphology and thus turbidity current flowpaths (Bernhardt et al., 2012; Corella et al., 2016).

Our study highlights the need to include fluid escape features in the MTD paleoseismic analysis, as was proposed by Moernaut et al. (2009). By doing so, we were able to construct a seismic event stratigraphy in Lake Calafquén that forms a complete representation of $M_w \geq 8.6$ earthquake recurrence, as is suggested by its one-to-one correlation with distal turbidites. However, a systematic comparative study of fluid escape features in different settings is needed to provide strict guidelines for their consistent identification and corresponding stratigraphic level. Moreover, this type of fluid escape features can only be used as positive evidence as they only exist above thick buried MTDs that are only occasionally formed.

6. Conclusions

We established, dated and compared a MTD stratigraphy for lakes Villarrica and Calafquén in the high-seismicity region of south-central Chile. We compared these MTD records with the average slope gradient of the landslide source areas, the position of major tephra layers in the slope sequences, and the results from previous geotechnical studies on slope stability in these lakes. This study resulted in the following general conclusions concerning recurrent landsliding and MTD stratigraphy, which may be applicable at other sedimentary basins in high-seismicity settings:

- Gentle slopes (<4°) allow the accumulation of thick sediment packages before reaching near-critical stability conditions, despite recurrent earthquake shaking. They therefore host the largest translational slides and have a higher potential for large landslide-induced tsunamis.
- Tephra layers can play a crucial role in the development of subaqueous translational failure. They are prone to liquefaction and act as a “weak layer” when they are shallowly buried, whereas liquefaction is unlikely when the tephra is buried under several meters of sediment. Repeated transfer of earthquake-induced excess pore pressure in the tephra towards the overlying unit may facilitate the development of a basal shear surface in the latter.
- The occurrence of voluminous landslides in a basin can follow a cyclic pattern. The early phase consists of the deposition of a tephra layer and the development of in-situ deformations directly on top. The end of the cycle is indicated by incipient scarp development once the slope sequence reaches a critical thickness. The landslide cycle can culminate in one major event, or a succession of large events due to scarp adjustments, retrogressive sliding and lateral debuttressing.
- The construction of an accurate MTD stratigraphy is subjected to limitations concerning the data type, the impact of landslides and MTDs on the overall stratigraphy and on operator bias. Generally, these factors lead to an underrepresentation of stratigraphic levels associated with MTDs, and can lead to incomplete MTD paleoseismic records in high-seismicity settings.

- MTD paleoseismology provides the best results at the base of relatively steep slopes (5-20°) subjected to frequent, minor landsliding. Implementation of fluid escape features and distal turbidites in the stratigraphic framework can strongly enhance the completeness of the paleoseismic record in high seismicity settings.

Acknowledgements

We thank the Chilean survey company BENTOS and the Flanders Marine Institute for the cost-effective logistical and technical support of the multibeam survey on Lake Villarrica and Calafquén, respectively. We thank the numerous persons that helped during the different multibeam, seismic and coring expeditions: Stephen Roberts, Anna Reusch, Alejandro Peña, François Charlet, Robert Brümmer, Rolf Kilian, Marcelo Arevalo, Javiera Cardenas, Francisco Martin, Koen De Rycker and Daniel Martínez. Wolfgang Recheis and Markus Erhardt are acknowledged for the acquisition of the medical CT-scans at the Innsbruck Medical University. We thank Michael Strasser and Karen Fontijn for fruitful discussions and Evelien Boes for graphic contributions on Fig. 12. IHS Markit is acknowledged for providing the Kingdom seismic interpretation software within their educational grant program. The contribution of J. Moernaut is funded via the Austrian Science Fund (FWF): project P30285-N34 and the Nachwuchsförderung 2016 of the University of Innsbruck. D. Melnick is supported by the Millennium Project CYCLO funded by ICM – MINECOM, Chile. R. Urrutia thanks the project CRHIAM/CONICYT/FONDAP/15130015. The contribution of M. De Batist and M. Van Daele is supported by the Research Foundation Flanders (FWO).

References

Beckers, A., Hubert-Ferrari, A., Beck, C., Papatheodorou, G., De Batist, M., Sakellariou, D., Tripsanas, E., Demoulin, A., 2018. Characteristics and frequency of large submarine landslides at the western tip of the Gulf of Corinth. Natural Hazards and Earth System Sciences 18, 1411-1425.

Bellwald, B., Hjelstuen, B.O., Sejrup, H.P., Haflidason, H., 2016. Postglacial mass movements and depositional environments in a high-latitude fjord system – Hardangerfjorden, Western Norway. Marine Geology 379, 157-175.

Bernhardt, A., Stright, L., Lowe, D.R., 2012. Channelized debris-flow deposits and their impact on turbidity currents: The Puchkirchen axial channel belt in the Austrian Molasse Basin. Sedimentology 59, 2042-2070.

Blaauw, M., Christen, J.A., 2011. Flexible paleoclimate age-depth models using an autoregressive gamma process. Bayesian Analysis 6, 457-474.

Brooks, G.R., 2016. Evidence of late glacial paleoseismicity from submarine landslide deposits within Lac Dasserat, northwestern Quebec, Canada. Quaternary Research 86(2), 184-199.

Chapron, E., Van Rensbergen, P., De Batist, M., Beck, C., Henriet, J.-P., 2004. Fluid-escape features as a precursor of a large sublacustrine sediment slide in Lake Le Bourget, NW Alps, France. Terra Nova 16, 305-311.

Cisternas, M., Atwater, B.F., Torrejon, F., Sawai, Y., Machuca, G., Lagos, M., Eipert, A., Youlton, C., Salgado, I., Kamataki, T., Shishikura, M., Rajendran, C.P., Malik, J.K., Rizal, Y., Husni, M., 2005. Predecessors of the giant 1960 Chile earthquake. Nature 437, 404-407.

Cisternas, M., Garrett, E., Wesson, R., Dura, T., Ely, L., 2017. Unusual geologic evidence of coeval seismic shaking and tsunamis shows variability in earthquake size and recurrence in the area of the giant 1960 Chile earthquake. Marine Geology 385, 101-113.

Clare, M.A., Chaytor, J., Dabson, O., Gamboa, D., Georgiopoulou, A., Eady, H., Hunt, J., Jackson, C., Katz, O., Krastel, S., Leon, R., Micallef, A., Moernaut, J., Moriconi, R., Moscardelli, L., Mueller, C., Normandeau, A., Patacci, M., Steventon, M., Urlaub, M., Voelker, D., Wood, L., Zane, J., 2018. A consistent global approach for the morphometric characterization of subaqueous landslides. Geological Society, London, Special Publications 477. doi:10.1144/SP477.15

Corella, J.P., Loizeau, J.-L., Kremer, K., Hilbe, M., Gerard, J., le Dantec, N., Stark, N., González-Quijano, M., Girardclos, S., 2016. The role of mass-transport deposits and turbidites in shaping modern lacustrine deepwater channels. Marine and Petroleum Geology 77, 515-525.

Dan, G., Sultan, N., Savoye, B., 2007. The 1979 Nice harbour catastrophe revisited: Trigger mechanism inferred from geotechnical measurements and numerical modelling. Marine Geology 245(1-4), 40-64.

Dura, T., Horton, B., Cisternas, M., Ely, L., Hong, I., Nelson, A., Wesson, R., Pilarczyk, J., Parnell, A., Nikitina, D., 2017. Subduction zone slip variability during the last millennium, south-central Chile. Quaternary Science Reviews 175, 112-137.

Fontijn, K., Lachowycz, S.M., Rawson, H., Pyle, D.M., Mather, T.A., Naranjo, J.-A., Moreno-Roa, H., 2014. Late Quaternary tephrostratigraphy of southern Chile and Argentina. Quaternary Science Reviews 89, 70-84.

Fontijn, K., Rawson, H., Van Daele, M., Moernaut, J., Abarzúa, A.M., Heirman, K., Bertrand, S., Pyle, D.M., Mather, T.A., De Batist, M., Naranjo, J.-A., Moreno, H., 2016. Synchronisation of sedimentary records using tephra: A postglacial tephrochronological model for the Chilean Lake District. Quaternary Science Reviews 137, 234-254.

Garga, V.K., McKay, L.D., 1984. Cyclic triaxial strength of mine tailings. Journal of Geotechnical Engineering 110(8), 19048. doi:10.1061/(ASCE)0733-9410(1984)110:8(1091)

Garrett, E., Shennan, I., Woodroffe, S.A., Cisternas, M., Hocking, E.P., Gulliver, P., 2015. Reconstructing paleoseismic deformation, 2: 1000 years of great earthquakes at Chucalén, south central Chile. Quaternary Science Reviews 113, 112-122.

Girardclos, S., Schmidt, O.T., Sturm, M., Ariztegui, D., Pugin, A., Anselmetti, F.S., 2007. The 1996 AD delta collapse and large turbidite in Lake Brienz. Marine Geology 241(1-4), 137-154.

Harders, R., Kutterolf, S., Hensen, C., Moerz, T., Brueckmann, W., 2010. Tephra layers: a controlling factor on submarine translational sliding? Geochemistry Geophysics Geosystems 11,Q05S23. doi:10.1029/2009GC002844

Heirman, K., 2011. A wind of change: Changes in position and intensity of the southern hemisphere westerlies during oxygen isotope stages 3, 2 and 1. PhD thesis, Ghent University, Belgium, 227 pp.

Hilbe, M., Anselmetti, F.S., 2015. Mass movement-induced tsunami hazard on perialpine Lake Lucerne (Switzerland): scenarios and numerical experiments. Pure and Applied Geophysics 172, 545-568.

Hogg, A.G., Hua, Q., Blackwell, P.G., Niu, M., Buck, C.E., Guilderson, T.P., Heaton, T.J., Palmer, J.G., Reimer, P.J., Reimer, R.W., Turney, C.S.M., Zimmerman, S.R.H., 2013. SHCal13 southern hemisphere calibration, 0–50,000 yr cal BP. Radiocarbon 55 (4), 1889-1903.

Hühnerbach, V., Masson, D.G., partners of the COSTA project, 2004. Landslides in the North Atlantic and its adjacent seas: an analysis of their morphology, setting and behaviour. Marine Geology 213 (1-4), 343-362.

Karlin, R.E., Holmes, M., Abella, S.E.B., Sylwester, R., 2004. Holocene landslides and a 3500-year record of Pacific Northwest earthquakes from sediments in Lake Washington. Geological Society of America Bulletin 116, 94e108. doi:10.1130/B25158.1.

Kempf, P., Moernaut, J., Van Daele, M., Vandoorne, W., Pino, M., Urrutia, R., De Batist, M., 2017. Coastal lake sediments reveal 5500 years of tsunami history in south central Chile. Quaternary Science Reviews 161, 99-116.

Kremer, K., Usman, M.O., Satoguchi, Y., Nagahashi, Y., Vadakkepuliyambatta, S., Panieri, G., Strasser, M., 2017a. Possible climate preconditioning on submarine landslides along a convergent margin, Nankai Trough (NE Pacific). Progress in Earth and Planetary Science 4(20). doi: 10.1186/s40645-017-0134-9

Kremer, K., Wirth, S.B., Reusch, A., Fäh, D., Bellwald, B., Anselmetti, F.S., Girardclos, S., Strasser, M., 2017b. Lake-sediment based paleoseismology: Limitations and perspectives from the Swiss Alps. Quaternary Science Reviews 168, 1-18.

Laugenie, C., 1982. La région des lacs, Chili meridional. PhD thesis, Université de Bordeaux III, Bordeaux, France.

L'Heureux, J.-S., Hansen, L., Longva, O., Eilertsen, R., 2013. Landslides along Norwegian fjords: causes and hazard assessment. Landslide Science and Practice: Complex Environment, 5, 81-87.

Locat, J., Lee, H.J., 2002. Submarine landslides: advances and challenges. Canadian Geotechnical Journal 39, 193-212.

Lomnitz, C., 1970. Major earthquakes and tsunamis in Chile during the period 1535 to 1955. Geologische Rundschau 59, 938-960.

McAdoo, B.G., Pratson, L.F., Orange, D.L., 2000. Submarine landslide geomorphology, US continental slope. Marine Geology 169 (1-2), 103-136.

Melnick, D., Charlet, F. Echtler, H.P., De Batist, M., 2006. Incipient axial collapse of the Main Cordillera and strain partitioning gradient between the central and Patagonian Andes, Lago Laja, Chile. Tectonics 25, TC5004. doi:10.1029/2005TC001918

Missiaen, T., Murphy, S., Loncke, L., Henriet, J.-P., 2002. Very high-resolution seismic mapping of shallow gas in the Belgian coastal zone. Continental Shelf Research 22, 2291-2301.

Moernaut, J., De Batist, M., 2011. Frontal emplacement and mobility of sublacustrine landslides: Results from morphometric and seismostratigraphic analysis. Marine Geology 285(1-4), 29-45.

Moernaut, J., De Batist, M., Charlet, F., Heirman, K., Chapron, E., Pino, M., Brummer, R., Urrutia, R., 2007. Giant earthquakes in South-Central Chile revealed by Holocene mass-wasting events in Lake Puyehue. Sedimentary Geology 195(3-4), 239-256.

Moernaut, J., De Batist, M., Heirman, K., Van Daele, M., Pino, M., Brümmer, R., Urrutia, R., 2009. Fluidization of buried mass-wasting deposits in lake sediments and its relevance for paleoseismology: Results from a reflection seismic study of lakes Villarrica and Calafquén (South-Central Chile). Sedimentary Geology 213, 121-135.

Moernaut, J., Van Daele, M., Heirman, K., Fontijn, K., Strasser, M., Pino, M., Urrutia, R., De Batist, M., 2014. Lacustrine turbidites as a tool for quantitative earthquake reconstruction: New evidence for a variable rupture mode in south central Chile. Journal of Geophysical Research – Solid Earth 119, 1607-1633.

Moernaut, J., Van Daele, M., Strasser, M., Clare, M.A., Heirman, K., Viel, M., Cardenas, J., Kilian, R., Ladrón de Guevara, B., Pino, M., Urrutia, R., De Batist, M., 2017a. Lacustrine turbidites produced by surficial slope sediment remobilization: a mechanism for continuous and sensitive turbidite paleoseismic records. Marine Geology 384, 159-176.

Moernaut, J., Wiemer, G., Reusch, A., Stark, N., De Batist, M., Urrutia, R., Ladrón de Guevara, B., Kopf, A., Strasser, M., 2017b. The influence of overpressure and focused fluid flow on subaquatic slope stability in a formerly glaciated basin: Lake Villarrica (South-Central Chile). Marine Geology 383, 35-54.

Moernaut, J., Van Daele, M., Fontijn, K., Heirman, K., Kempf, P., Pino, M., Valdebenito, G., Urrutia, R., Strasser, M., De Batist, M., 2018. Larger earthquakes recur more periodically: New insights in the megathrust

earthquake cycle from lacustrine turbidite records in south-central Chile. Earth and Planetary Science Letters 481, 9-19.

Mohamad, R., Dobry, R., 1986. Undrained monotonic and cyclic triaxial strength of sand. Journal of Geotechnical Engineering 112(10), 941-958.

Moreno, H., Toloza, V., 2015. The large tephra fall deposits related to the ca. 3500 BP Pucón eruption: an unexpected revelation, Villarrica volcano, Southern Andes 39.4°S, Chile. Proceedings of the XIV Congreso Geológico Chileno (October 2015, La Serena, Chile) 1(3), 570-573.

Moreno, M.S., Bolte, J., Klotz, J., Melnick, D., 2009. Impact of megathrust geometry on inversion of coseismic slip from geodetic data: Application to the 1960 Chile earthquake. Geophysical Research Letters 36, L16310. doi:10.1029/2009GL039276

Moreno, M., Li, S., Melnick, D., Bedford, J. R., Baez, J.C., Motagh, M., Metzger, S., Vajedian, S., Sippl, C., Gutknecht, B.D., Contreras-Reyes, E., Deng, Z., Tassara, A., Oncken, O., 2018. Chilean megathrust earthquake recurrence linked to frictional contrast at depth. Nature Geoscience 11, 285-290.

Moscardelli, L., Wood, L., 2016. Morphometry of mass-transport deposits as a predictive tool. Geological Society of America Bulletin, 128, 47-80.

Mosher, D.C., Monahan, P.A., Barrie, J.V., Courtney, R.C., 2004. Coastal submarine failures in the Strait of Georgia, British Columbia: Landslides of the 1946 Vancouver Island Earthquake. Journal of Coastal Research 20(1), 277-291.

Obermeier, S.F., 1996. Use of liquefaction-induced features for paleoseismic analysis – An overview of how seismic liquefaction features can be distinguished from other features and how their regional distribution and properties of source sediment can be used to infer the location and strength of Holocene paleo-earthquakes. Engineering Geology 44, 1-76.

Parsons, T., Geist, E.L., Ryan, H.F., Lee, H.J., Haeussler, P.J., Lynett, P., Hart, P.E., Sliter, R., Roland, E., 2014. Source and progression of a submarine landslide and tsunami: The 1964 Great Alaska earthquake at Valdez. Journal of Geophysical Research – Solid Earth 119, 8502-8516.

Pinson, L.J.W., Vardy, M.E., Dix, J.K., Henstock, T.J., Bull, J.M., Maclachlan, S.E., 2013. Deglacial history of glacial Lake Windermere, UK: implications for the central British and Irish ice sheet. Journal of Quaternary Science 28(1), 83-94.

Pope, E.L., Talling, P.J., Carter, L., 2017. Which earthquakes trigger damaging submarine mass movements: Insights from a global record of submarine cable breaks? Marine Geology 384, 131-146.

Praet, N., Moernaut, J., Van Daele, M., Boes, E., Haeussler, P.J., Strupler, M., Schmidt, S., Loso, M.G., De Batist, M., 2017. Paleoseismic potential of sublacustrine landslide records in a high-seismicity setting (south-central Alaska). Marine Geology 384, 103-119.

Puzrin, A.M., Gray, T.E., Hill, A.J., 2015. Significance of the actual nonlinear slope geometry for catastrophic failure in submarine landslides. Proceedings of the Royal Society A 471, 20140772. doi:10.1098/rspa.2014.0772

Sammartini, M., Camerlenghi, A., Budillon, F., Insinga, D.D., Zgur, F., Conforti, A., Iori, M., Romeo, R., Tonielli, R., 2018. Open-slope, translational submarine landslide in a tectonically active volcanic continental margin (Licosa submarine landslide, southern Tyrrhenian Sea). Geological Society, London, Special Publications, 477. doi:10.1144/SP477.34

Sammartini, M., Moernaut, J., Anselmetti, F.S., Hilbe, M., Lindhorst, K., Praet, N., Strasser, M., in press. An atlas of mass-transport deposits in lakes, in: Ogata, K., Pini, G.A., Festa, A.(Eds.), Submarine Landslides: Subaqueous Mass Transport Deposits from Outcrops to Seismic Profiles, Geophysical Monograph Series - AGU Books.

Sawyer, D.E., DeVore, J.R., 2015. Elevated shear strength of sediments on active margins: Evidence for seismic strengthening. Geophysical Research Letters 42, 10216-10221,

Schanmugam, G., 2015. The landslide problem. Journal of Palaeogeography 4(2), 109-166.

Schnellmann, M., Anselmetti, F.S., Giardini, D., McKenzie, J.A., Ward, S.N., 2002. Prehistoric earthquake history revealed by lacustrine slump deposits. Geology 30(12), 1131-1134.

SHOA (Servicio Hidrográfico y Oceanográfico de la Armada de Chile), 1987. Lago Villarrica, scale 1:40000, Santiago, Chile.

SHOA (Servicio Hidrográfico y Oceanográfico de la Armada de Chile), 2008. Lago Calafquén, scale 1:30000, Santiago, Chile.

Smith, S.B., Karlin, R.E., Kent, G.M., Seitz, G.G., Driscoll, N.W., 2013. Holocene subaqueous paleoseismology of Lake Tahoe. Geological Society of America Bulletin 125 (5-6), 691-708.

Silva Parejas, C., Druitt, T.H., Robin, C., Moreno, H., Naranjo, J.A., 2010. The Holocene Pucón eruption of Volcán Villarrica, Chile: deposit architecture and eruption chronology. Bulletin of Volcanology 72(6), 677-692.

Strasser, M., Anselmetti, F.S., Fäh, D., Giardini, D., Schnellmann, M., 2006. Magnitudes and source areas of large prehistoric northern alpine earthquakes revealed by slope failures in lakes. Geology 34(12), 1005-1008.

Strasser, M., Hilbe, M., Anselmetti, F.S., 2011. Mapping basin-wide subaquatic slope failure susceptibility as a tool to assess regional seismic and tsunami hazards. Marine Geophysical Research 32(1-2), 331-347.

Strozyk, F., Strasser, M., Förster, A., Kopf, A., Huhn, K., 2010. Slope failure repetition in active margin environments: Constraints from submarine landslides in the Hellenic fore arc, eastern Mediterranean. Journal of Geophysical Research 115, B08103. doi:10.1029/2009JB006841

Strupler, M., Anselmetti, F.S., Hilbe, M., Strasser, M., 2018. Quantitative characterization of subaqueous landslides in Lake Zurich (Switzerland) based on a high-resolution bathymetric dataset. In: Lintern, D. G.,Mosher, D. C., Moscardelli, L. G., Bobrowsky, P. T., Campbell, C., Chaytor, J. D., Clague, J. J., Georgiopoulou, A., Lajeunesse, P., Normandeau, A., Piper, D. J. W., Scherwath, M., Stacey,C., Turmel, D. (Eds.) Subaqueous Mass Movements. Geological Society, London, Special Publications 477. doi: 10.1144/SP477.7

Sumner, E.J., Siti, M.I., McNeill, L.C., Talling, P.J., Henstock, T.J., Wynn, R.B., Djajadihardja, Y.S., Permana, H., 2013. Can turbidites be used to reconstruct a paleoearthquake record for the central Sumatran margin? Geology 41, 763-766.

Talling, P.J., Clare, M.A., Urlaub, M., Pope, E., Hunt, J.E., Watt, S.F., 2014. Large submarine landslides on continental slopes: geohazards, methane release, and climate change. Oceanography, 27, 32-45.

Tappin, D. R., Watts, P., McMurtry, G. M., Lafoy, Y., Matsumoto, T., 2001. The Sissano, Papua New Guinea tsunami of July 1998 – Offshore evidence on the source mechanism, Marine Geology 175, 1-23.

ten Brink, U.S., Andrews, B.D., Miller, N.C., 2016. Seismicity and sedimentation rate effects on submarine slope stability. Geology 44(7), 563-566.

Urlaub, M., Talling, P.J., Masson, D.G., 2013. Timing and frequency of large submarine landslides: implications for understanding triggers and future geohazard. Quaternary Science Reviews 72, 63-82.

Urlaub, M., Talling, P.J., Zervos, A., Masson, D., 2015. What causes large submarine landslides on low gradient (<2°) continental slopes with slow (~0.15 m/kyr) sediment accumulation? Journal of Geophysical Research - Solid Earth 120, 6722-6739.

Van Daele, M., Moernaut, J., Silversmit, G., Schmidt, S., Fontijn, K., Heirman, K., Vandoorne, W., De Clercq, M., Van Acker, J., Wolff, C., Pino, M., Urrutia, R., Roberts, S.J., Vincze, L., De Batist, M., 2014. The 600 yr eruptive history of Villarrica Volcano (Chile) revealed by annually laminated lake sediments. Geological Society of America Bulletin 126(3-4), 481-498.

Van Daele, M., Moernaut, J., Doom, L., Boes, E., Fontijn, K., Heirman, K., Vandoorne, W., Hebbeln, D., Pino, M., Urrutia, R., Brümmer, R., De Batist, M., 2015. A comparison of the sedimentary records of the 1960 and 2010 great Chilean earthquakes in 17 lakes: implications for quantitative lacustrine paleoseismology. Sedimentology 62(5), 1466-1496.

Vardy, M.E., Vanneste, M., Henstock, T.J., Clare, M.A., Forsberg, C.F., Provenzano, G., 2017. State-of-the-art remote characterization of shallow marine sediments: the road to a fully integrated solution. Near Surface Geophysics 15, 387-402.

Völker, D., Scholz, F., Geersen, J., 2011. Analysis of submarine landsliding in the rupture area of the 27 February 2010 Maule earthquake, Central Chile. Marine Geology 288(1-4), 79-89.

Waldmann, N., Anselmetti, F.S., Ariztegui, D., Austin, J.A., Pirouz, M., Moy, C.M., Dunbar, R., 2011. Holocene mass-wasting events in Lago Fagnano, Tierra del Fuego (54S): implications for paleoseismicity of the Magallanes–Fagnano transform fault. Basin Research 23 (2), 171-190.

Wiemer, G., Kopf, A., 2016. On the role of volcanic ash deposits as preferential submarine slope failure planes. Landslides 14(1). doi:10.1007/s10346-016-0706-6

Wiemer, G., Moernaut, J., Stark, N., Kempf, P., De Batist, M., Pino, M., Urrutia, R., Strasser, M., Kopf, A., 2015. The role of sediment composition and behavior under dynamic loading conditions on slope failure initiation: a study of a subaqueous landslide in earthquake-prone South-Central Chile. International Journal of Earth Sciences 104(5), 1439-1457.

Zobin, V.M., 2001. Seismic hazard of volcanic activity, Journal of Volcanology and Geothermal Research 112, 1-14.

Table captions

Table 1: Event stratigraphy of Lake Villarrica and Calafquén, including MTD events, cored turbidites and fluid escape events on seismic profiles.

Table 2: Types of methodological uncertainties associated with MTD stratigraphy, its implications for paleoseismic research and possible method improvements.

Figure captions

Fig.1: A) Setting of the studied lakes in South-Central Chile with indication of the rupture areas of the AD 1960 (M_w 9.5) and AD 2010 (M_w 8.8) megathrust earthquakes. B) Local morphological setting of lakes Villarrica and Calafquén with indication of river network. General lake bathymetry is based on interpolation of data points of SHOA (1987) and SHOA (2008) with contour lines every 50 m. C and D) Multibeam bathymetry map of the studied basins in Lake Villarrica (C) and Lake Calafquén (D). Location of basins is indicated on (B). Light grey squares: main coring sites; dark grey square: secondary coring site.

Fig.2: A) Pinger profile in Lake Villarrica with indication of mass-transport deposits (MTDs) () and their corresponding stratigraphic levels. Note the erosive features under the large MTDs and the fluid escape

structures (vertical acoustic wipe-out) above them. B) Overview pinger profile linking the three main coring sites (VILL1, VILL3 and VILL4). R1 and R2 are marker tephras. Note the gas blanking under MTD-F. C) Location of the seismic profiles in Lake Villarrica shown in this article. The full seismic grid is presented in SI-Fig. 1. Bathymetric contours every 5 m.

Fig. 3: MTD stratigraphy of Lake Villarrica illustrated by MTD distribution maps for different seismic horizons. For clarity, we only mention the weighted mean age of each event (see also Table 1).

Fig. 4: A) Core-to-seismic correlation of core VILL3 to a sparker profile. The MTD events on the seismic stratigraphy are shown as letters and colored arrows, the turbidites and MTDs in the cores as numbers. The values of γ-density are in g cm^{-3} and those of magnetic susceptibility (MagSus) in 10^{-5} SI. The full core log and detailed legend of VILL3 is presented in SI-Fig. 2. The detailed core-to-seismic correlation of the upper 9 m is presented in SI-Fig.4. B) Event-free age-depth model of VILL3.

Fig. 5: A) Core-to-seismic correlation of core VILL4 to a pinger profile. Symbols and colors as in Fig. 4A. The full core details are in SI-Fig. 3. B) Event-free age-depth model of VILL4. Symbols and colors as in Fig. 4B.

Fig. 6: A) Location of cores VILL1 and VILLAR1. B) Core-to-seismic correlation of VILL1. Large peaks in density correspond to strong reflections on the pinger profile. C) Event-free age-depth model of VILL1. D) Pinger profile crossing VILLAR1 showing the seismic facies correlation with a (condensed) cut-out of the seismic profile at VILL1. R1 and R2 serve as marker horizons. E) Core-to-seismic correlation of VILLAR1 as presented in Wiemer et al. (2015). Density peaks associated with major tephra layers correspond to strong reflections.

Fig. 7: A) Pinger profile in Lake Calafquén with indication of MTDs and their corresponding stratigraphic levels. Location and orientation of profiles are on the bathymetric map inset. B and C) Pinger profiles crossing the gully related to event MTD-M (in green; see Fig. 8). Purple MTDs relate to local side-wall failures of the gully. D) Upslope pinger profile showing a buried headscarp produced by landslide event M which developed on top of horizon R2. The post-failure sediment drape exhibits thin sliding/slumping on top of R2, and a thick incipient scarp reaching the lakefloor. The inset figure shows the comparable seismic facies succession between VILL1 and the presented profile (right end of profile: purple dashed lines) with the presence of the R2 reflection. The seismic cut-out from VILL1 (see Fig. 6) was condensed to account for possible differences in sedimentation rate between sites.

Fig. 8: MTD stratigraphy of Lake Calafquén illustrated by MTD distribution maps for different seismic horizons. Upper left corner: slope gradient map of the SW portion of the basin showing landslide scarps and MTDs. For the MTD events, we only mention the weighted mean age of each event (see also Table 1). Symbols and color coding as in Fig. 3 (red: outline of MTD; pink square: turbidite in core CAL1; green cross: level not reached by CAL1 core). For event M, we indicate the inferred transport directions (orange arrows), headscarps (black line), frontal ramps (dashed black line), and the associated gully formation in the basin (white transparent zone).

Fig. 9: A) Core-to-seismic correlation of core CAL1 to a pinger profile. The MTD events on the seismic stratigraphy are shown as letters and colored arrows, the turbidites and MTDs in the cores as numbers. B) Event-free age-depth model of CAL1 (modified after Moernaut et al., 2018).

Fig. 10: Volume and average slope angle of landslides in Villarrica (blue triangles) and Calafquén (red squares). A power law regression line on each data set was drawn for visual reference. Note the logarithmic scale for landslide volume. Landslide volume was estimated using pinger profiles crossing the MTDs (see section 3). The slope angle is the average value of the failed slope segment. The pie-charts illustrate the relative distribution of MTD volume per lake. Total volume (100%) is 19.3 x 10^6 m^3 in Villarrica; 10.1 x 10^6 m^3 in Calafquén.

Fig. 11: Stratigraphic position of tephra with respect to sediment deformations and slope failures. A) Pinger profile illustrating differently-sized deformations developed above R1: i) thin deformations (<1 m) during event J; thick deformations (~4 m) during event F. Location of pinger profiles on Fig. 2C. B) Comparison between deformed glacio-lacustrine sediments south of Lago Laja (see also Melnick et al., 2006) and deformed sediments in a section of VILL1. In both cases, the plastic sediment deformations are directly underlain by a sandy tephra layer. C) Comparison of the R2 tephra and overlaying sediments of an intact sequence with in-situ deformation (core VILLAR8) and a failed sequence during landslide event F (cores VILLAR3/5). The greyscale images represent CT-scan data (darker: lower CT number). D) Upslope pinger profile showing the intact sequence above R2 at coring site VILLAR8 (see C). Slope failure occurred higher up in the stratigraphy and is discussed in Moernaut et al. (2017b). E) Upslope pinger profile showing the main headscarp and missing slope sections (at coring sites VILLAR3/5; see C) evacuated during landslide event F (see Wiemer et al., 2015).

Fig. 12: A) Flow-chart summarizing the influence of near-surface tephra and deeper buried tephra on the possible development of liquefaction, sediment deformations and landsliding during strong seismic shaking.

B) Conceptual model of the build-up of a gently-dipping sedimentary sequence containing sandy tephra layers and which is frequently impacted by strong earthquakes causing in-situ deformation and finally slope failure. Model based on the sequence at VILLAR1 and VILL1.

Fig. 13: The subaqueous landslide cycle in Lake Villarrica (blue triangles) and Calafquén (red squares), since the deposition of tephra R2. Grey zones indicate the age of tephra R2 and R1.

Fig. 14: Temporal comparison and correlation of the event stratigraphy in Villarrica and Calafquén, including MTDs, turbidites and fluid escape events. Light grey rectangles represent the age range of possible temporal correlations between events in the two lakes. The dark grey rectangle is the Pucón volcanic event (Tephra R1). The three oldest events (M-K) in Villarrica are poorly mapped due to limitations in seismic penetration ("poor seismics"). The age of events N-R in Calafquén is obtained by extrapolation of the age-depth model in CAL1 and therefore these ages are poorly constrained.

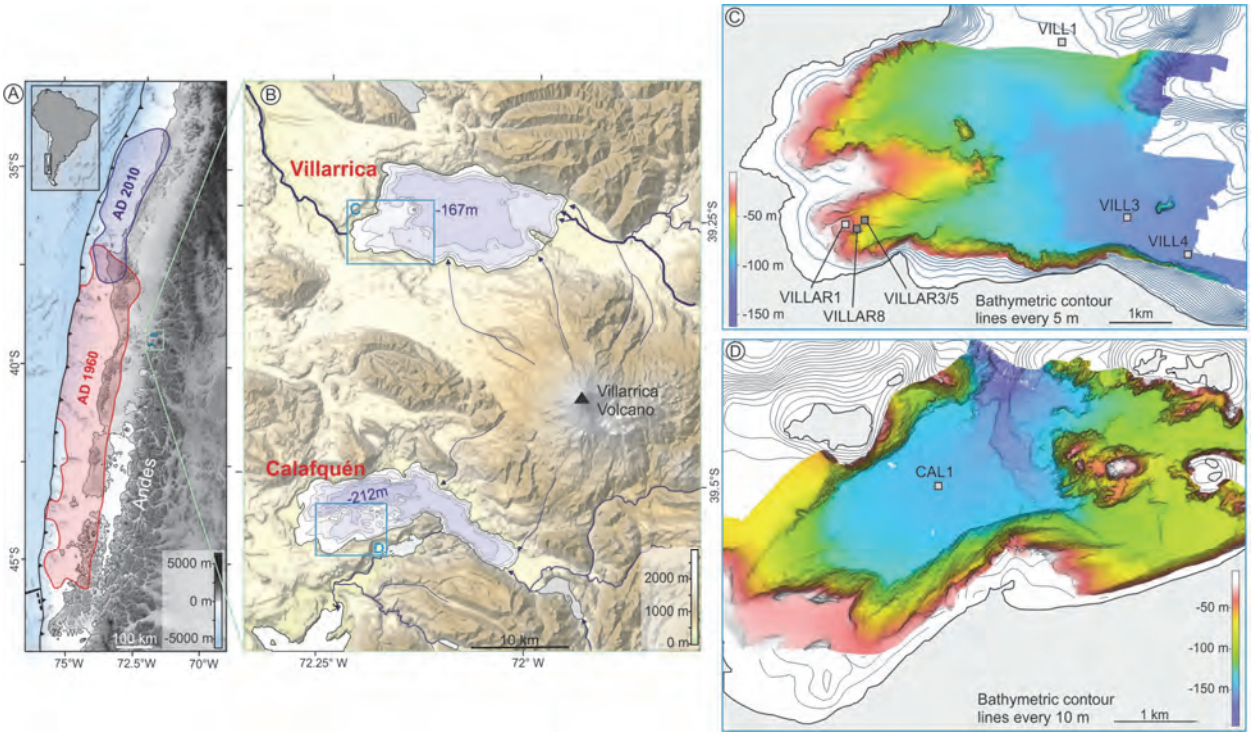
A
B
C
D
AD 2010
AD 1960
Andes
35°S
40°S
45°S
75°W
72.5°W
70°W
5000 m
0 m
-5000 m
100 km
Villarrica
-167m
Calafquén
-212m
Villarrica Volcano
72.25° W
72° W
39.25°S
39.5°S
2000 m
1000 m
0 m
10 km
VILL1
VILL3
VILL4
-50 m
-100 m
-150 m
VILLAR1
VILLAR8
VILLAR3/5
Bathymetric contour lines every 5 m
1km
CAL1
Bathymetric contour lines every 10 m
1 km

Fig. 1

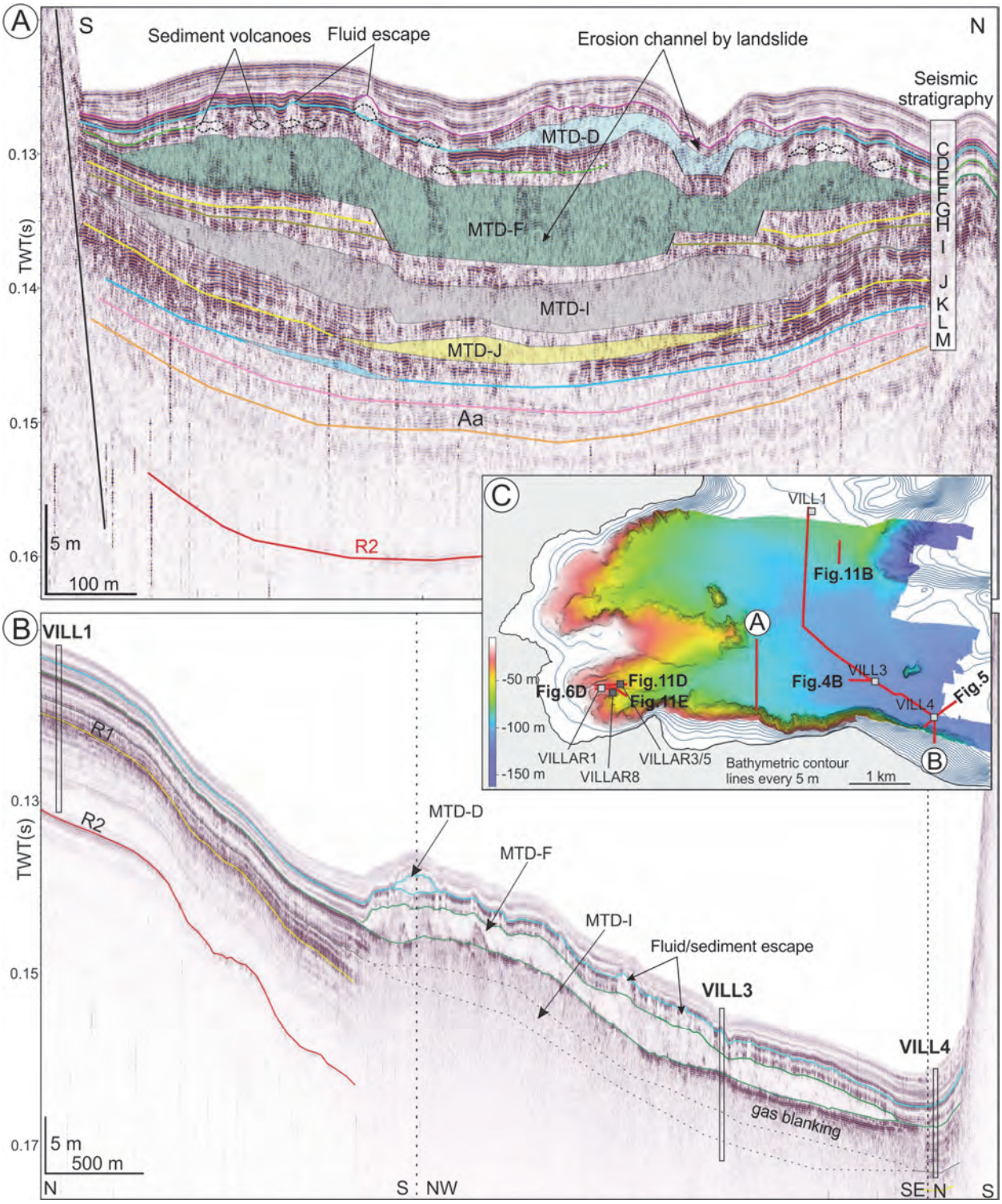
A
S
N
Sediment volcanoes
Fluid escape
Erosion channel by landslide
Seismic stratigraphy
C D E F G H I J K L M
MTD-D
MTD-F
MTD-I
MTD-J
Aa
R2
TWT(s)
0.13
0.14
0.15
0.16
5 m
100 m
C
VILL1
Fig.11B
A
-50 m
-100 m
-150 m
Fig.6D
Fig.11D
Fig.11E
Fig.4B
VILL3
VILL4
Fig.5
VILLAR1
VILLAR8
VILLAR3/5
Bathymetric contour lines every 5 m
1 km
B
B
VILL1
R1
R2
MTD-D
MTD-F
MTD-I
Fluid/sediment escape
VILL3
VILL4
gas blanking
0.13
0.15
0.17
5 m
500 m
N
S
NW
SE
N
S

Fig. 2

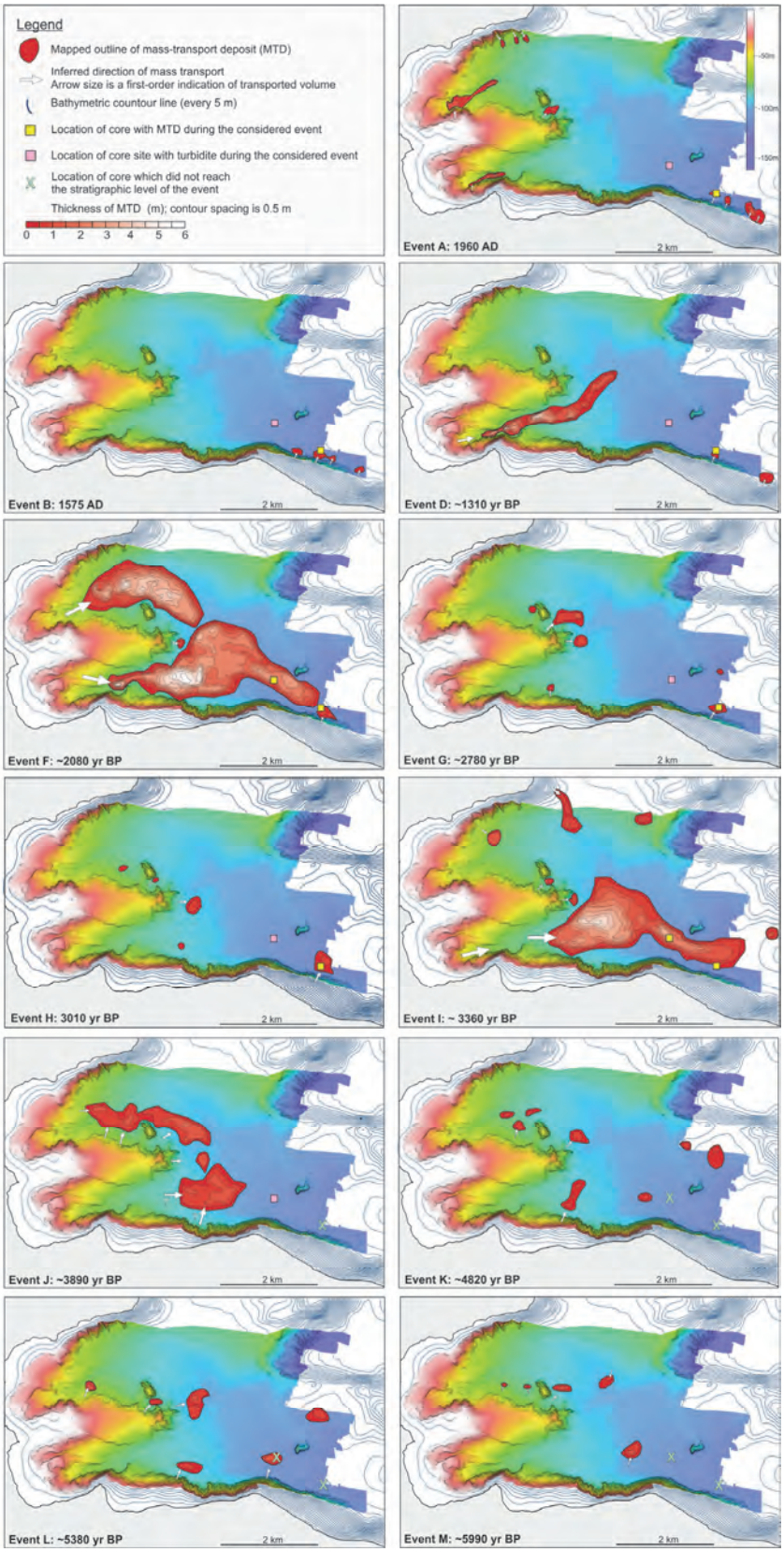

Fig. 3 (split in two parts)

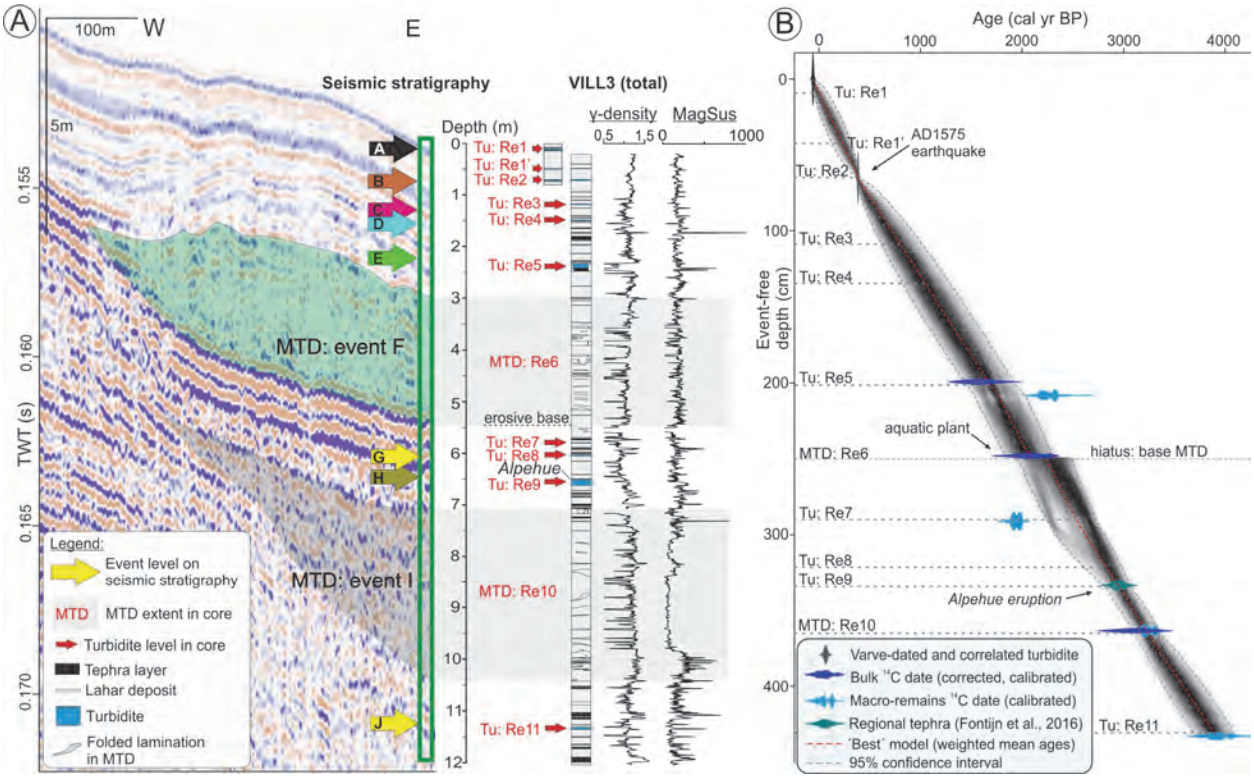
A
100m
W
E
Seismic stratigraphy
VILL3 (total)
γ-density
MagSus
Depth (m)
5m
TWT (s)
MTD: event F
MTD: event I
Legend:
Event level on seismic stratigraphy
MTD extent in core
Turbidite level in core
Tephra layer
Lahar deposit
Turbidite
Folded lamination in MTD
Tu: Re1
Tu: Re1'
Tu: Re2
Tu: Re3
Tu: Re4
Tu: Re5
MTD: Re6
erosive base
Tu: Re7
Tu: Re8
Alpehue
Tu: Re9
MTD: Re10
Tu: Re11
B
Age (cal yr BP)
Event-free depth (cm)
AD1575 earthquake
aquatic plant
hiatus: base MTD
Alpehue eruption
Varve-dated and correlated turbidite
Bulk 14C date (corrected, calibrated)
Macro-remains 14C date (calibrated)
Regional tephra (Fontijn et al., 2016)
'Best' model (weighted mean ages)
95% confidence interval

Fig. 4

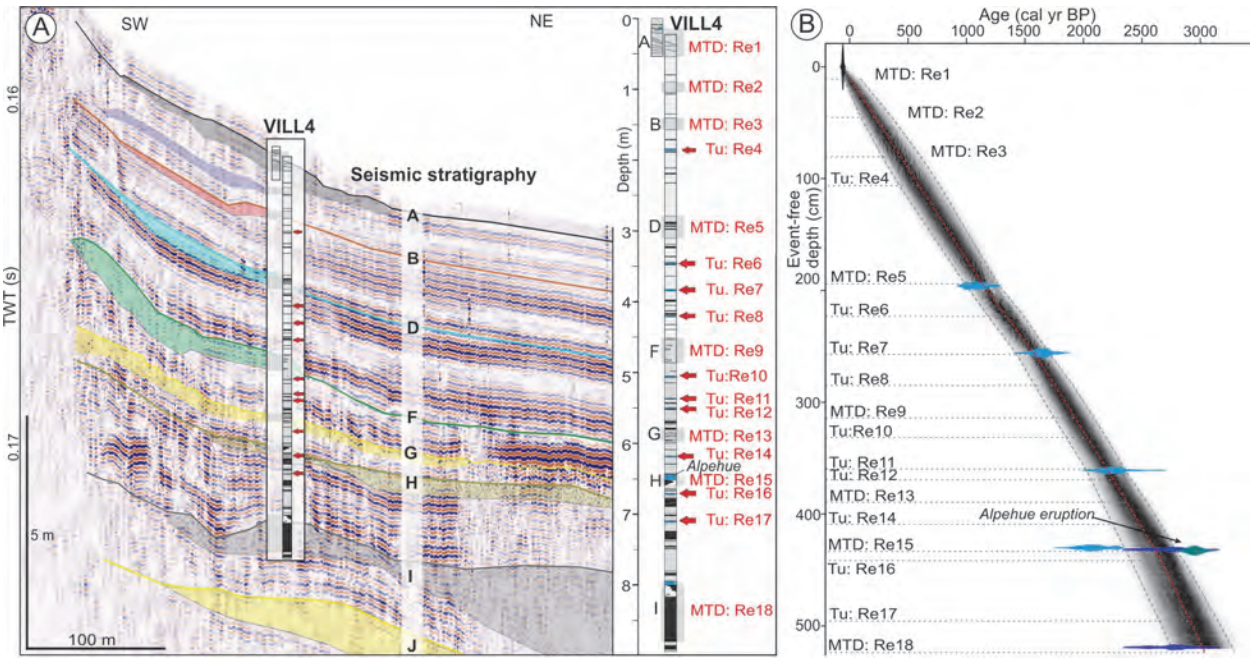
A
SW
NE
VILL4
Seismic stratigraphy
TWT (s)
Depth (m)
5 m
100 m
MTD: Re1
MTD: Re2
MTD: Re3
Tu: Re4
MTD: Re5
Tu: Re6
Tu. Re7
Tu: Re8
MTD: Re9
Tu:Re10
Tu: Re11
Tu: Re12
MTD: Re13
Tu: Re14
Alpehue
MTD: Re15
Tu: Re16
Tu: Re17
MTD: Re18
B
Age (cal yr BP)
Event-free depth (cm)
Alpehue eruption

Fig. 5

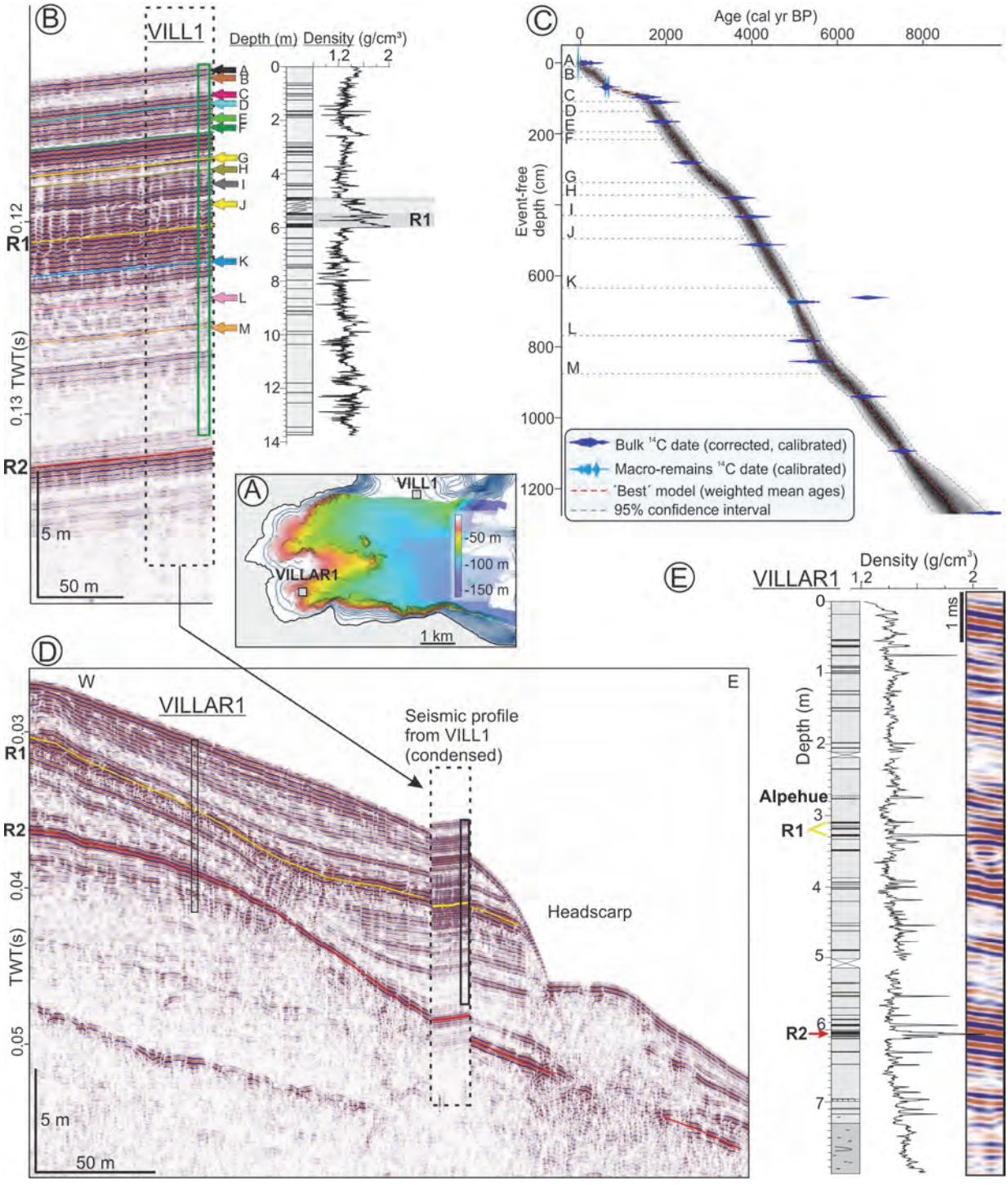
B
VILL1
Depth (m) Density (g/cm³)
1,2
2
R1
R2
0,12
0,13 TWT(s)
5 m
50 m
A
VILL1
VILLAR1
-50 m
-100 m
-150 m
1 km
C
Age (cal yr BP)
0
2000
4000
6000
8000
Event-free depth (cm)
Bulk ¹⁴C date (corrected, calibrated)
Macro-remains ¹⁴C date (calibrated)
´Best´ model (weighted mean ages)
95% confidence interval
D
W
E
VILLAR1
Seismic profile from VILL1 (condensed)
Headscarp
0,03
0,04
0,05
TWT(s)
5 m
50 m
E
VILLAR1
Density (g/cm³)
1,2
2
1 ms
Depth (m)
Alpehue
R1
R2

Fig. 6

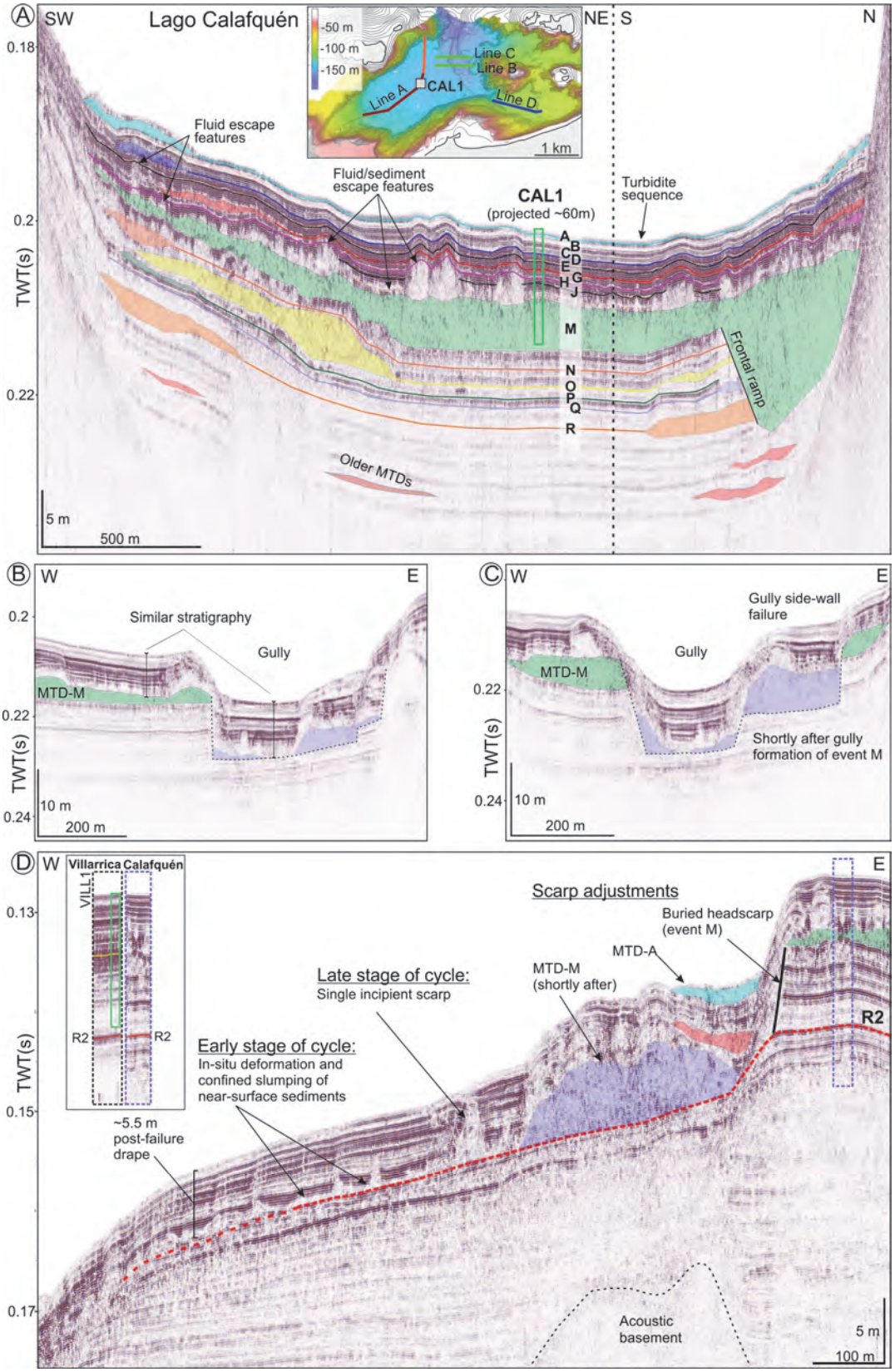
A
SW
Lago Calafquén
NE
S
N
-50 m
-100 m
-150 m
Line A
CAL1
Line C
Line B
Line D
1 km
Fluid escape features
Fluid/sediment escape features
CAL1
(projected ~60m)
Turbidite sequence
TWT(s)
0.18
0.2
0.22
A
B
C
D
E
G
H
J
M
N
O
P
Q
R
Frontal ramp
Older MTDs
5 m
500 m
B
W
E
Similar stratigraphy
Gully
MTD-M
0.2
0.22
0.24
TWT(s)
10 m
200 m
C
W
E
Gully side-wall failure
Gully
MTD-M
Shortly after gully formation of event M
0.22
0.24
TWT(s)
10 m
200 m
D
W
Villarrica Calafquén
VILL1
R2
R2
E
Scarp adjustments
Buried headscarp (event M)
MTD-A
MTD-M (shortly after)
Late stage of cycle:
Single incipient scarp
Early stage of cycle:
In-situ deformation and confined slumping of near-surface sediments
R2
~5.5 m post-failure drape
TWT(s)
0.13
0.15
0.17
Acoustic basement
5 m
100 m

Fig. 7

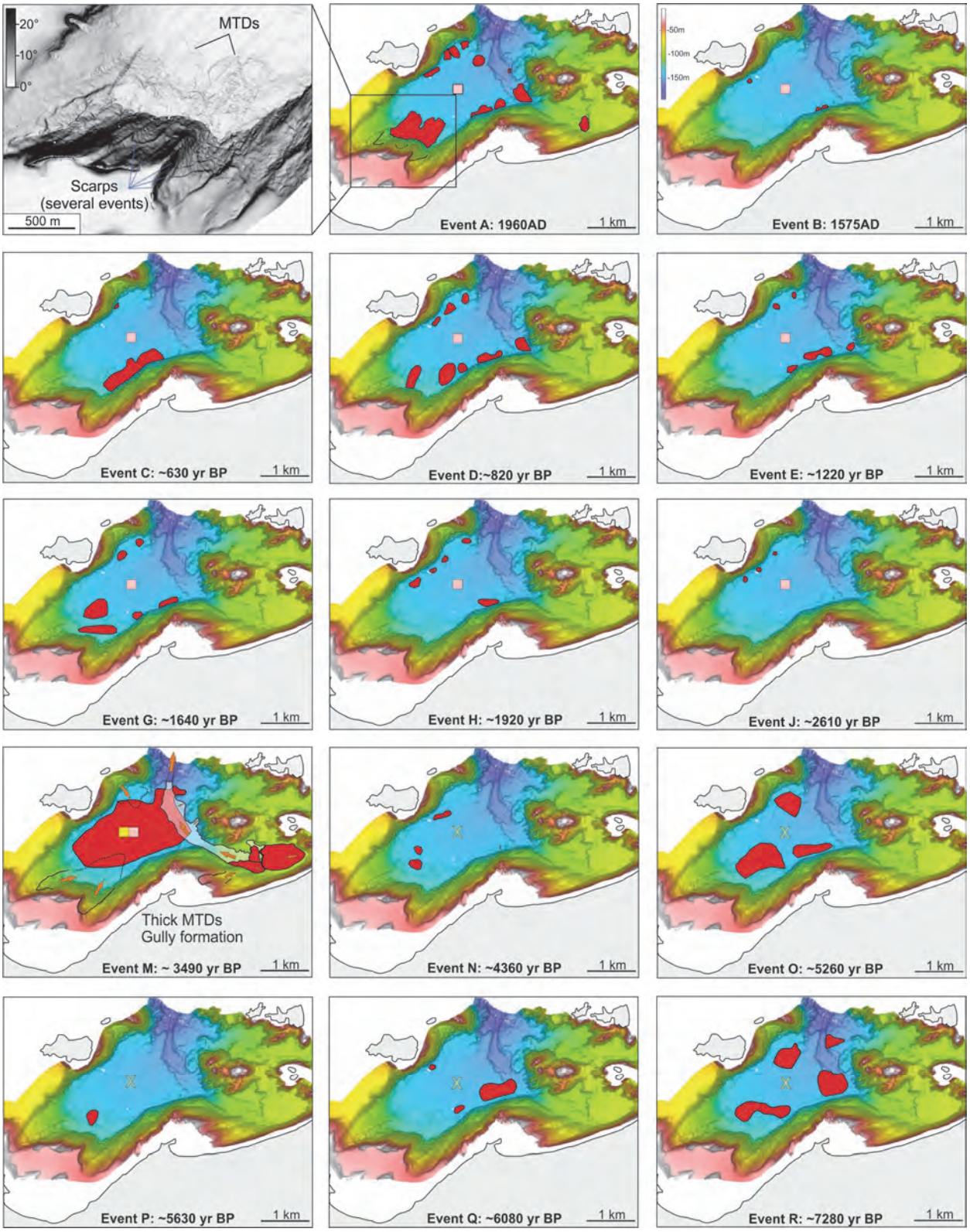
20°
10°
0°
MTDs
Scarps
(several events)
500 m
Event A: 1960AD
1 km
-50m
-100m
-150m
Event B: 1575AD
1 km
Event C: ~630 yr BP
1 km
Event D:~820 yr BP
1 km
Event E: ~1220 yr BP
1 km
Event G: ~1640 yr BP
1 km
Event H: ~1920 yr BP
1 km
Event J: ~2610 yr BP
1 km
Thick MTDs
Gully formation
Event M: ~ 3490 yr BP
1 km
Event N: ~4360 yr BP
1 km
Event O: ~5260 yr BP
1 km
Event P: ~5630 yr BP
1 km
Event Q: ~6080 yr BP
1 km
Event R: ~7280 yr BP
1 km

Fig. 8

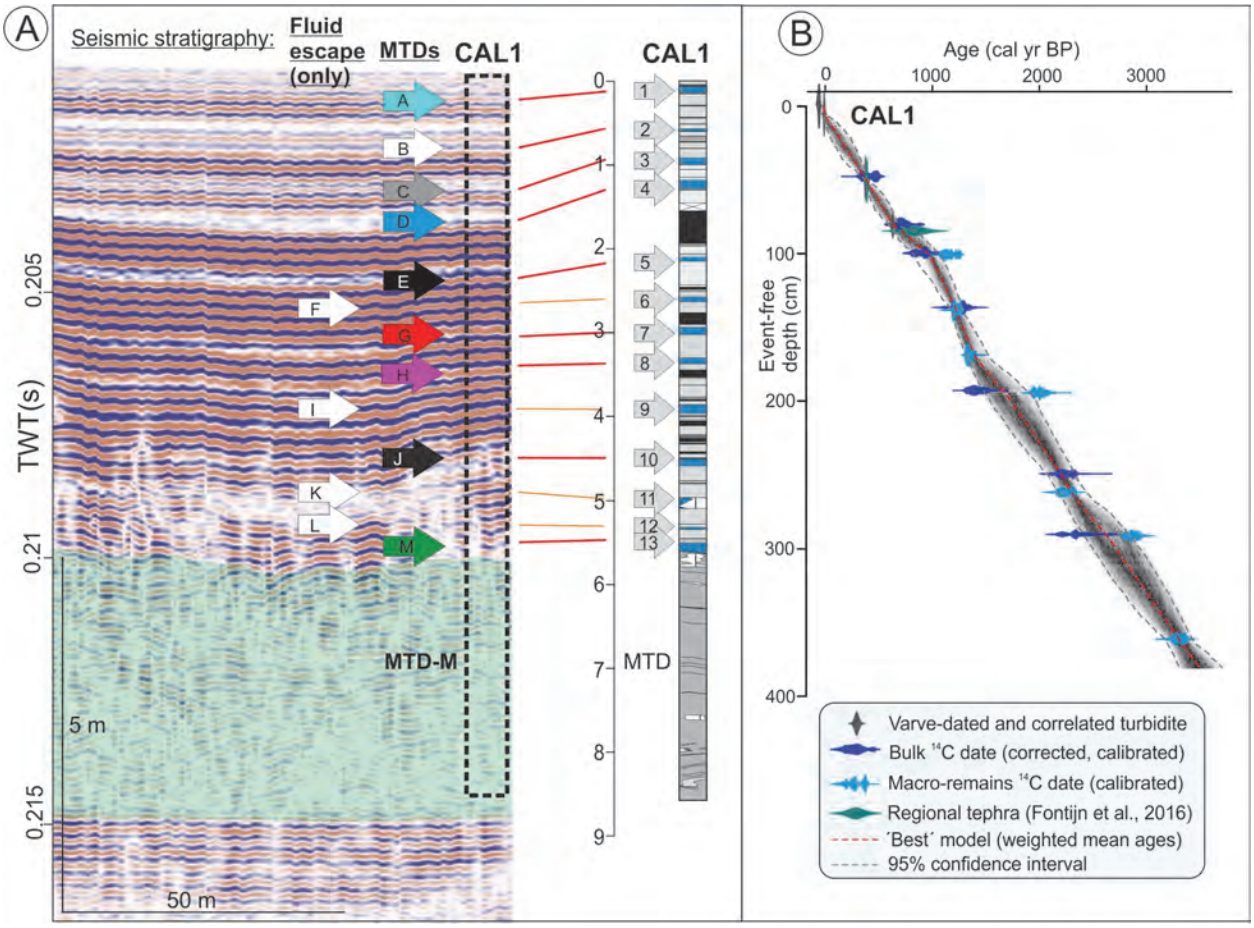
A
Seismic stratigraphy:
Fluid escape (only)
MTDs
CAL1
CAL1
TWT(s)
0,205
0,21
0,215
MTD-M
5 m
50 m
MTD
B
Age (cal yr BP)
0
1000
2000
3000
CAL1
Event-free depth (cm)
100
200
300
400
Varve-dated and correlated turbidite
Bulk 14C date (corrected, calibrated)
Macro-remains 14C date (calibrated)
Regional tephra (Fontijn et al., 2016)
´Best´ model (weighted mean ages)
95% confidence interval

Fig. 9

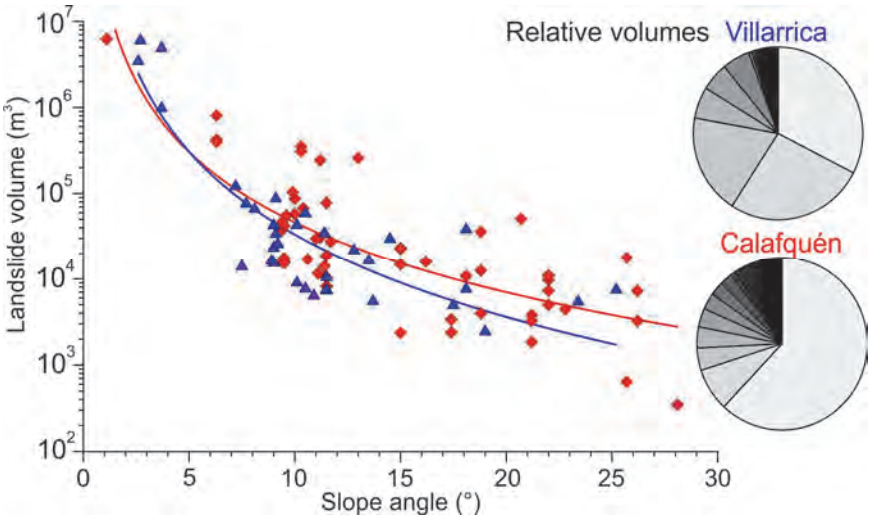
Relative volumes
Villarrica
Calafquén
Landslide volume (m3)
Slope angle (°)

Fig. 10

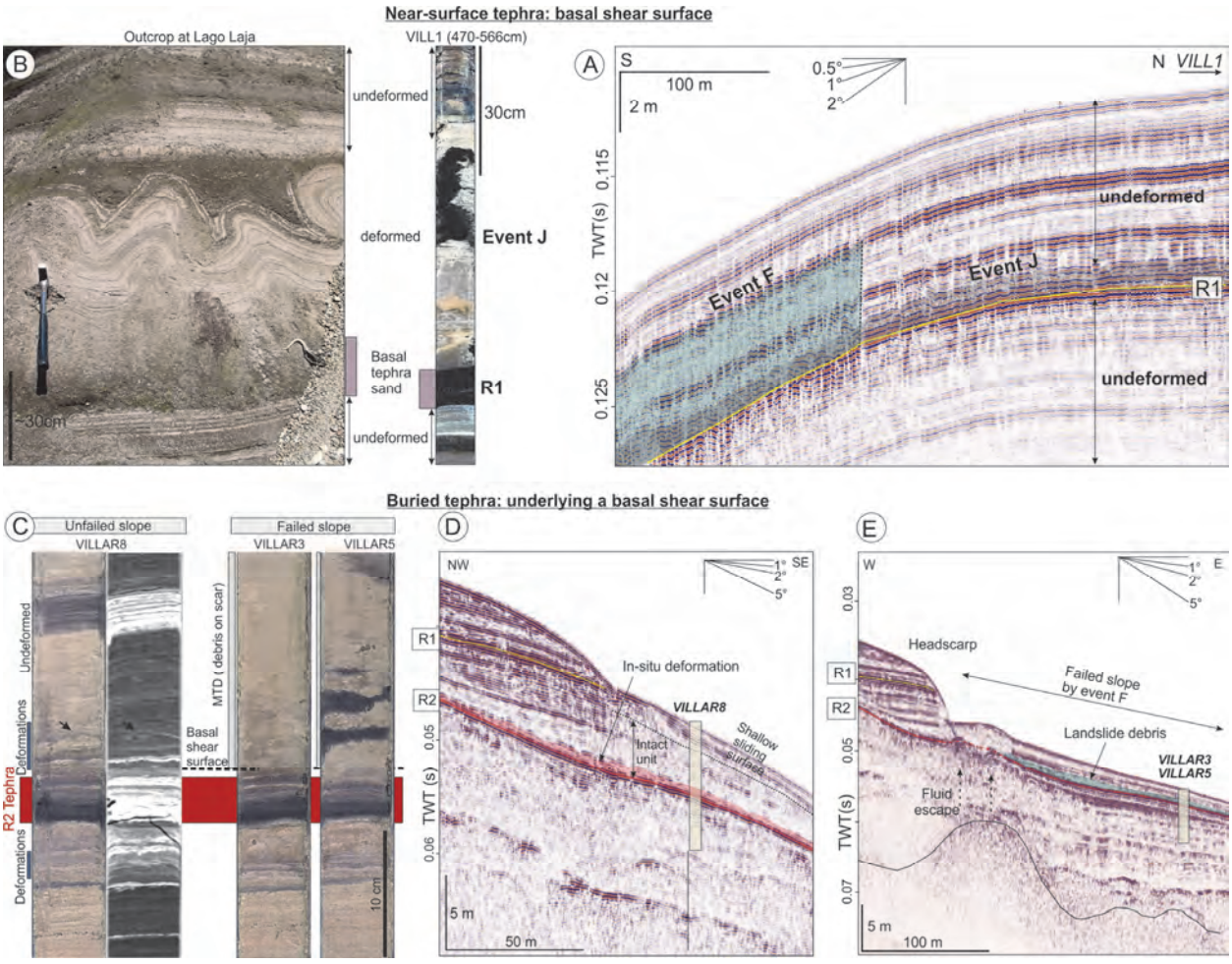
Near-surface tephra: basal shear surface
Outcrop at Lago Laja
B
VILL1 (470-566cm)
undeformed
30cm
deformed
Event J
Basal tephra sand
R1
undeformed
~30cm
A
S
N VILL1
100 m
2 m
0.5°
1°
2°
0.115
TWT(s)
0.12
0.125
undeformed
Event F
Event J
R1
undeformed
Buried tephra: underlying a basal shear surface
C
Unfailed slope
Failed slope
VILLAR8
VILLAR3
VILLAR5
Undeformed
Deformations
R2 Tephra
Deformations
MTD (debris on scar)
Basal shear surface
10 cm
D
NW
SE
1°
2°
5°
R1
R2
In-situ deformation
VILLAR8
Intact unit
Shallow sliding surface
0.05
TWT (s)
0.06
5 m
50 m
E
W
E
1°
2°
5°
0.03
Headscarp
R1
R2
Failed slope by event F
Landslide debris
VILLAR3
VILLAR5
0.05
Fluid escape
TWT(s)
0.07
5 m
100 m

Fig. 11

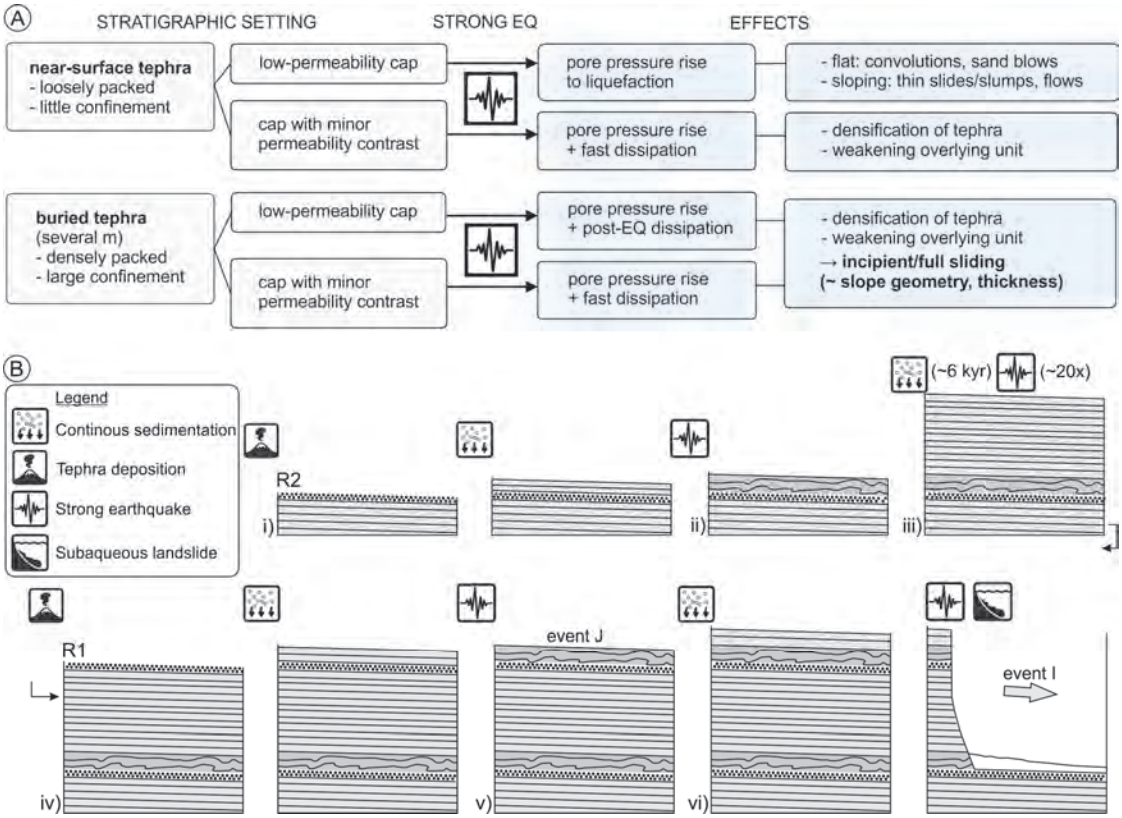

Fig. 12

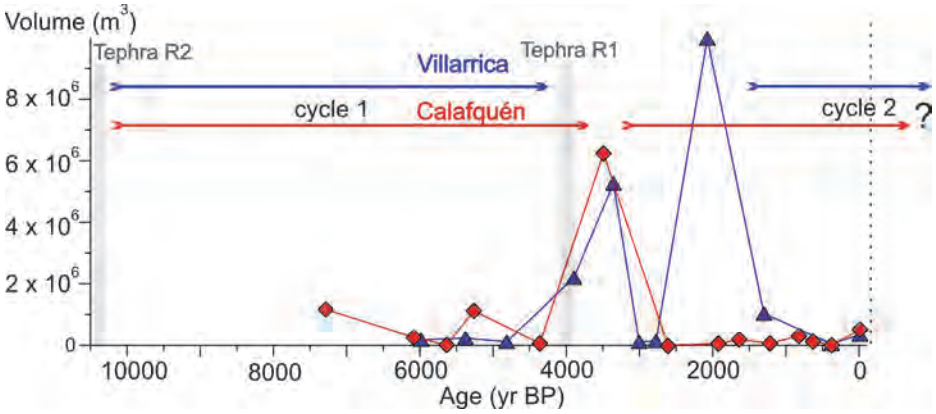

Fig. 13

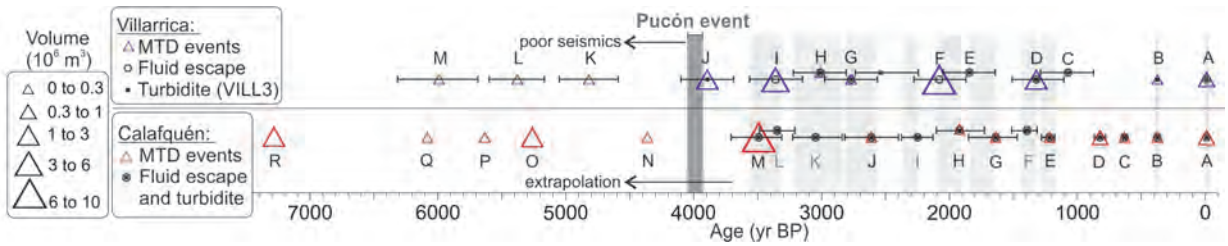

Fig. 14

The subaqueous landslide cycle in south-central Chilean lakes: the role of tephra, slope gradient and repeated seismic shaking

Moernaut, J., Van Daele, M., Heirman, K., Wiemer, G., Molenaar, A., Vandorpe, T., Melnick, D., Hajdas, I., Pino, M., Urrutia, R., De Batist, M.

Supplementary figures

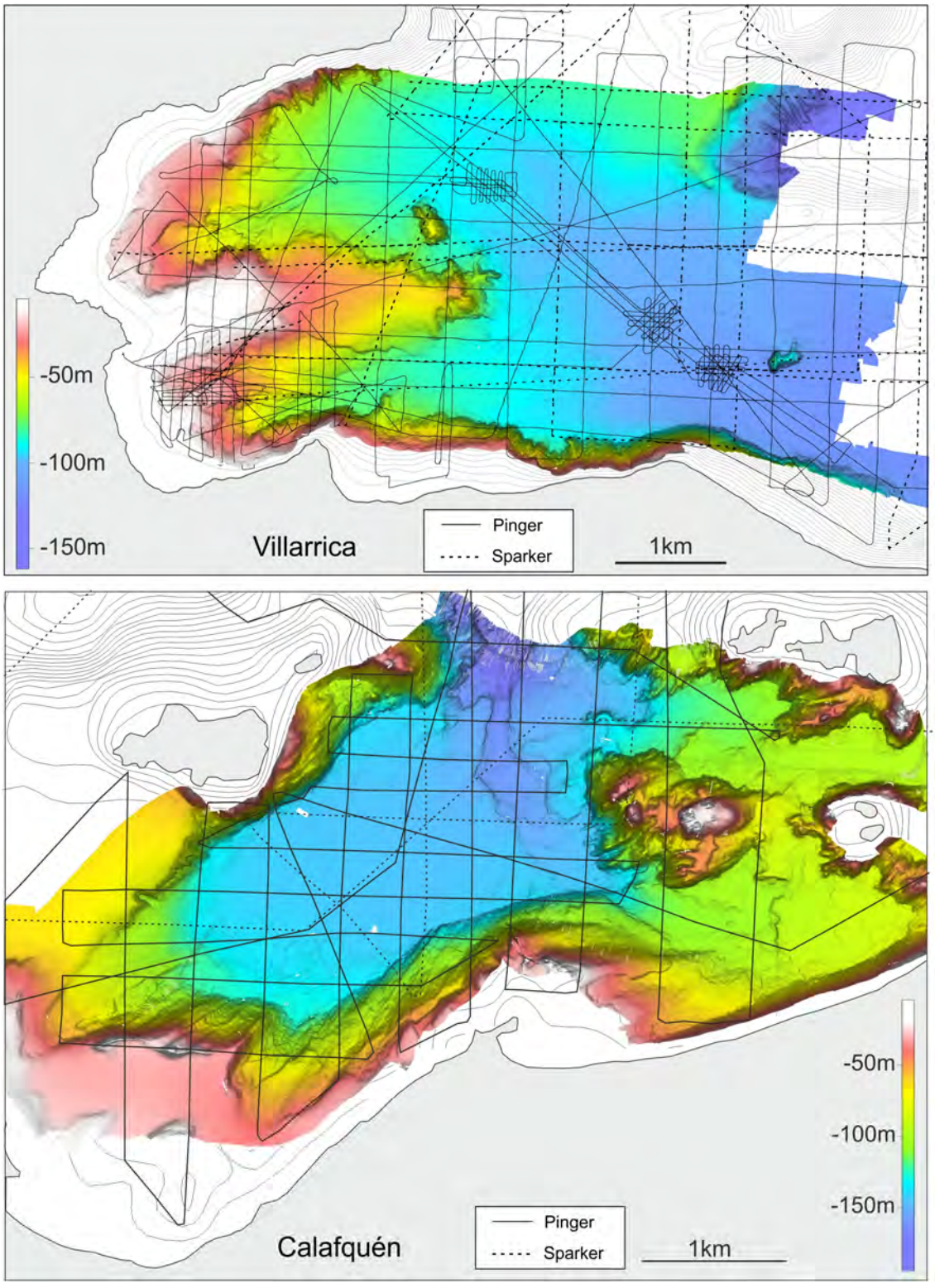

Si-Fig. 1: Reflection seismic survey grids in lakes Villarrica (above) and Calafquén (below) on the multibeam bathymetry maps. Details of the pinger and sparker systems can be found in section 3.

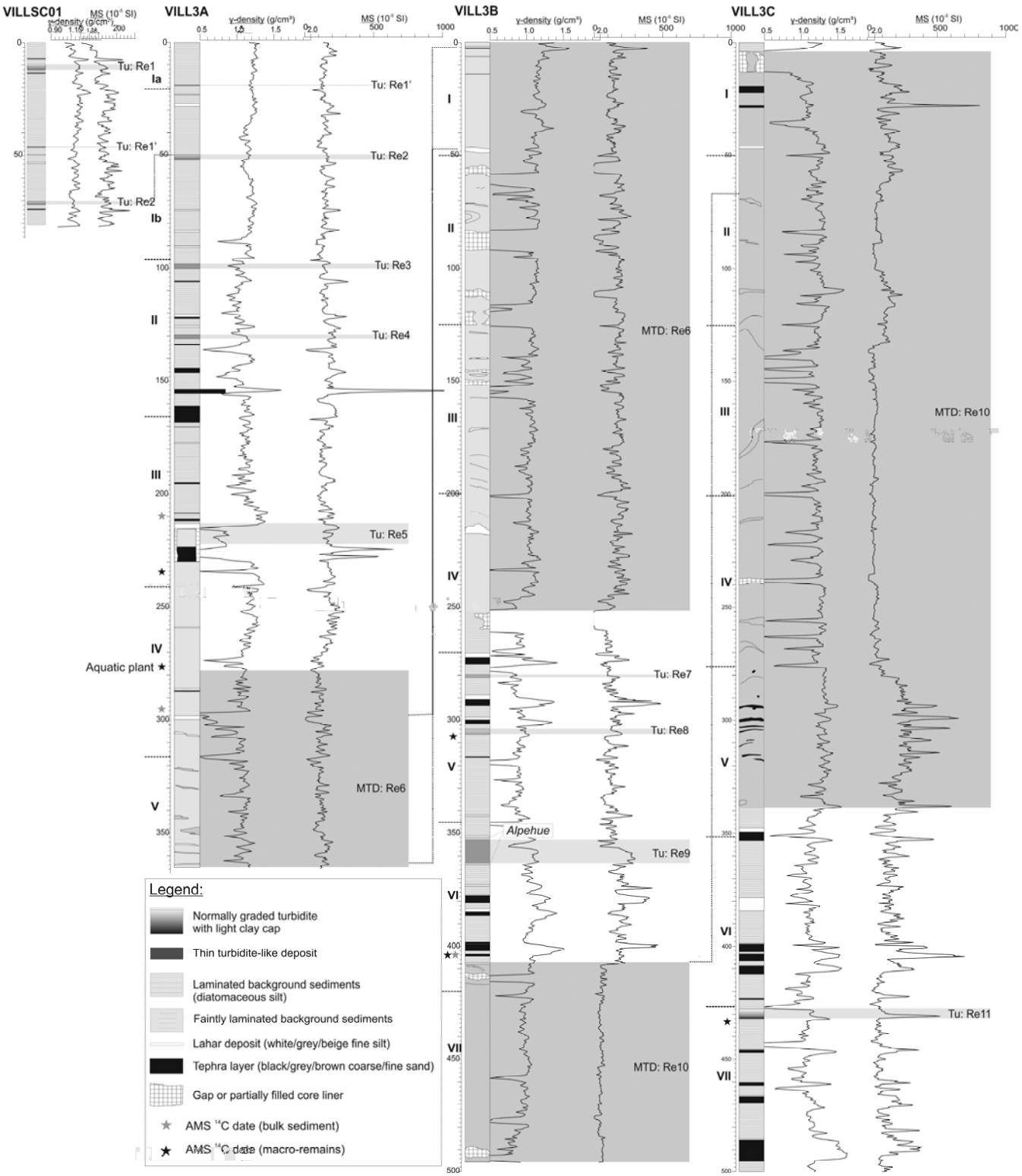

Si-Fig. 2: Detailed lithological log of the core segments of VILL3 (see legend) with indication of magnetic susceptibility, γ-density and locations of radiocarbon samples. Troughs in γ-density are caused by cracks in the sediments and partly-filled liners. Peaks in MagSus are associated with deposits of volcanic origin (tephra, lahars) or with a thin sandy base of lacustrine turbidites (Tu).

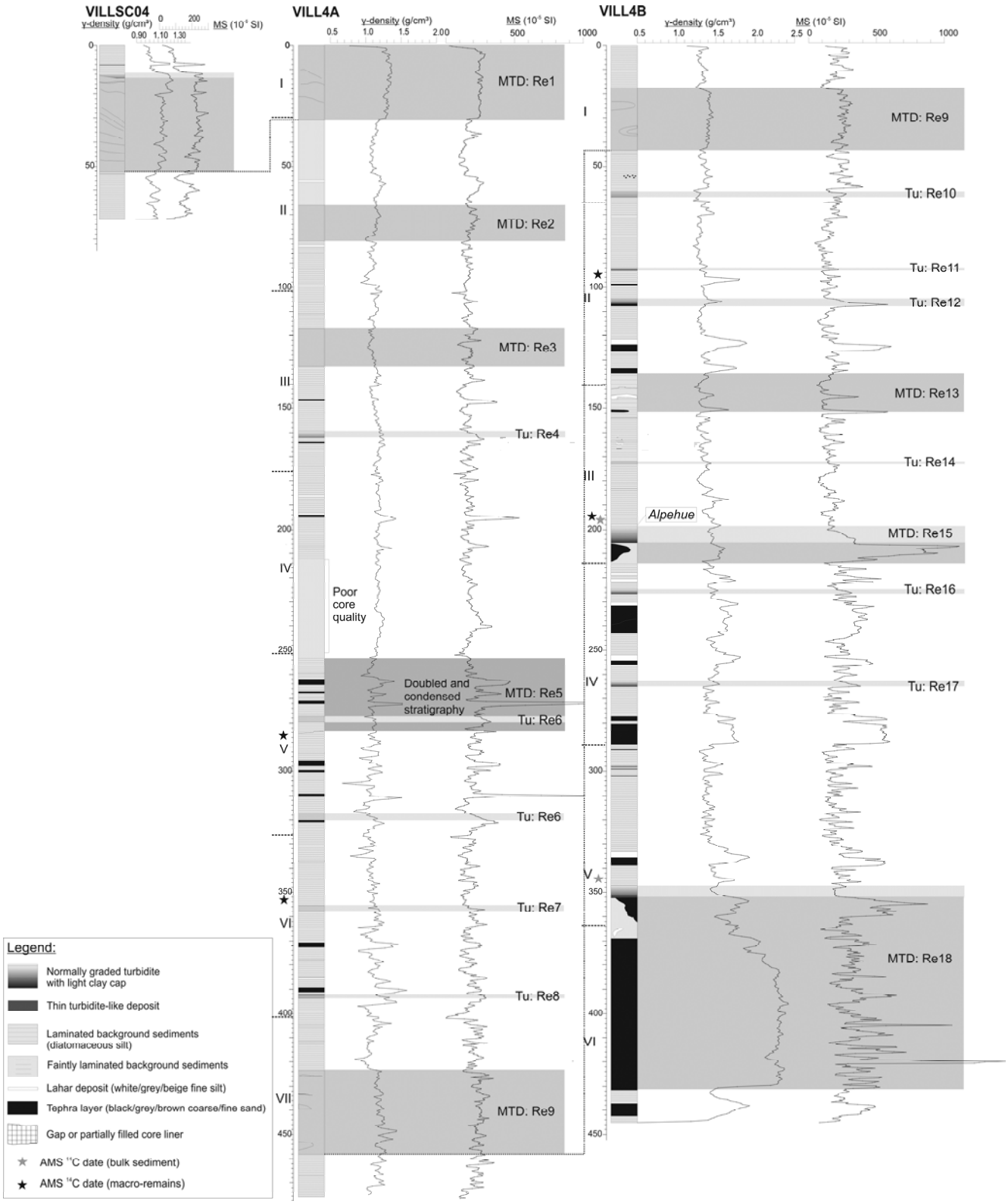

Si-Fig. 3: Detailed lithological log of the core segments of VILL4 (see legend) with indication of magnetic susceptibility, γ-density and locations of radiocarbon samples. Troughs in γ-density are caused by cracks in the sediments and partly-filled liners. Peaks in MagSus are associated with deposits of volcanic origin (tephra, lahars) or with a thin sandy base of lacustrine turbidites (Tu).

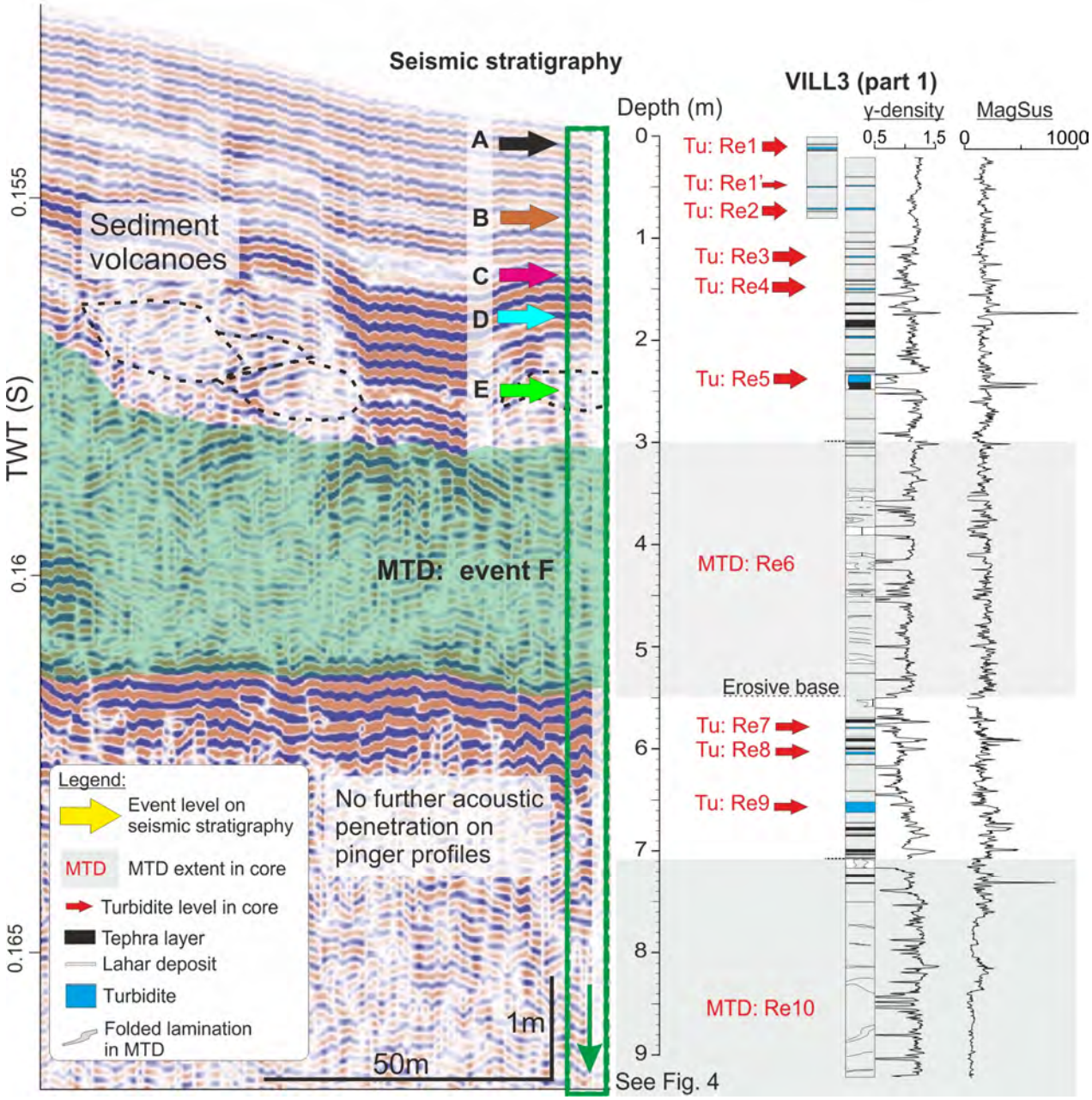

Si-Fig. 4: A) Core-to-seismic correlation of core VILL3 (upper 9 m) to a pinger profile. The MTD events on the seismic stratigraphy are shown as letters and colored arrows, the turbidites and MTDs in the cores as numbers. The values of γ-density are in g/cm^3 and those of magnetic susceptibility (MagSus) in 10^{-5} SI. The full core log and detailed legend of VILL3 is presented in SI-Fig. 2.

VILLARRICA

MTD level on seismics	Depth in core VILL1 (cm)	Event-free depth in VILL1 (cm)	Min. Age (yr BP)	Max. Age (yr BP)	"Best" Age (yr BP)	Dating info	Volume total (m^3)	Presence in VILL3	Presence in VILL4	Fluid escape level?
A	10	10	-10	-10	-10	1960 EQ	351780	Tu: Re1	MTD: Re1	yes
B	40	40	375	375	375	1575 EQ	43520	Tu: Re2	MTD: Re3	maybe
D	137	135.6	1103	1515	1309	average	1033850	Tu: Re4	MTD: Re5	yes
F	221	214.9	1874	2286	2080	average	9977420	MTD: Re6	MTD: Re9	yes
G	344	335.8	2572	2984	2778	average	143160	Tu: Re 8	MTD: Re13	yes
H	380	371.1	2804	3216	3010	average	107225	Tu: Re 9	MTD: Re15	yes
I	439	428	3157	3569	3363	average	5267880	MTD: Re10	MTD: Re18	yes
J	520	493	3697	4090	3894	VILL3	2196550	Tu: Re11	Not cored	poor data
K	728	633.3	4592	5052	4821	VILL1	117150	Not cored	Not cored	poor data
L	863	765	5168	5600	5380	VILL1	233570	Not cored	Not cored	poor data
M	973	871.8	5688	6314	5991	VILL1	185200	Not cored	Not cored	poor data

Fluid escape levels without mapped MTDs	Depth in core VILL1 (cm)	Event-free depth in VILL1 (cm)	Min. Age (yr BP)	Max. Age (yr BP)	"Best" Age (yr BP)	Dating info	Presence in VILL3	Presence in VILL4
C	110	108.6	872	1284	1078	average	Tu: Re3	x
E	200	193.9	1640	2052	1846	average	Tu: Re5	Tu: Re 8

Turbidites in VILL3 without mapped MTDs or fluid escape	Depth in core VILL3 (cm)	Event-free depth in VILL3 (cm)	Min. Age (yr BP)	Max. Age (yr BP)	"Best" Age (yr BP)	Dating info	Presence in VILL4
Tu: Re1´	46	42.5	213	213	229	1737 EQ	MTD: Re2
Tu: Re7	611	290.3	2239	2730	2532	VILL3	Tu: Re12

Turbidites in VILL4 without mapped MTDs or fluid escape	Depth in core VILL3 (cm)	Event-free depth in VILL4 (cm)	Min. Age (yr BP)	Max. Age (yr BP)	"Best" Age (yr BP)	Dating info
Tu: Re4	182	106.1	425	772	595	VILL4
Tu: Re6	341	223	1184	1490	1341	VILL4
Tu: Re7	378	257	1429	1713	1586	VILL4
Tu: Re10	448	331.3	1750	2089	1928	VILL4
Tu: Re11	530	359.5	2019	2352	2201	VILL4
Tu: Re14	610	408.9	2250	2662	2484	VILL4
Tu: Re16	663	441.3	2406	2859	2665	VILL4
Tu: Re17	751	495.5	2650	3151	2912	VILL4

CALAFQUEN

MTD level (seismics)	Depth in core CAL1 (cm)	Event-free depth (cm)	Min. Age (yr BP)	Max. Age (yr BP)	"Best" Age (yr BP)	Dating info	Volume total (m^3)	Presence in CAL1	Fluid escape level?
A	5.7	5.6	-10	-10	-10	1960 EQ	508890	Tu: Re1	yes
B	57.1	49.6	375	375	375	1575 EQ	4328	Tu: Re2	yes
C	91.5	81.2	622	640	631	CAL1	124300	Tu: Re3	yes
D	118.5	98.6	779	867	823	CAL1	304150	Tu: Re4	yes
E	211.4	137.5	1177	1282	1218	CAL1	64900	Tu: Re5	yes
G	296.7	192.3	1471	1852	1638	CAL1	190660	Tu: Re7	yes
H	333.3	220.1	1724	2103	1923	CAL1	56820	Tu: Re8	yes
J	453.6	289.4	2399	2819	2611	CAL1	4890	Tu: Re10	yes
M	556.9	380	3311	3708	3492	CAL1	6235900	MTD + Tu:	yes
N					4362	Extrap.	62540	Not cored	Poor data
O					5262	Extrap.	1118400	Not cored	Poor data
P					5634	Extrap.	14040	Not cored	Poor data
Q					6082	Extrap.	257980	Not cored	Poor data
R					7282	Extrap.	1162940	Not cored	Poor data

Fluid escape levels without mapped MTDs	depth in core CAl1 (cm)	Event-free depth (cm)	Min. Age (yr BP)	Max. Age (yr BP)	"Best" Age (yr BP)	Dating info	Presence in CAL1
F	254.9	168.4	1315	1514	**1395**	CAL1	Tu: Re 6
I	389.6	256	2130	2376	**2251**	CAL1	Tu: Re 9
K	501	334.2	2840	3226	**3048**	CAL1	Tu: Re 11
L	538.8	365.3	3209	3485	**3348**	CAL1	Tu: Re 12

Limiting factor for MTD stratigraphy	Possible effect on MTD stratigraphy	Possible effect on paleoseismic record	Method improvements
Vertical resolution of subbottom profiles	- Missing out thin MTDs - Wrongly assigning MTDs to the same stratigraphic level	- Missing earthquakes of small impact on sediment archive - Overestimation of sedimentary impact of certain earthquakes	- Processing: deconvolution on high-quality seismic data - More sediment cores to detect thin MTDs - Evaluate MTD stratigraphy by comparison with turbidite records from distal cores
MTDs not covered by survey lines	Missing out small MTDs	- Missing earthquakes of small impact on sediment archive - Underestimation of sedimentary impact of certain earthquakes	- Denser survey grids at the foot of slope based on detailed (paleo-)bathymetry - High-resolution 3D seismics and post-processing
Decrease in seismic penetration/quality with subsurface depth. Gas blanking.	- More recent events seem to have a larger impact than the older events - High-quality MTD stratigraphy restricted to last few millennia	Underrepresentation of the presence and/or impact of older events	- Complement subbottom profiles with lower-frequency reflection seismic data. Thin MTDs remain undetected - Careful assessment of data quality with depth
Repeated sliding in a short time span	Difficulties to discriminate individual MTDs. Older events may be undetected	Underrepresentation of the presence and/or impact of older events	Evaluate MTD stratigraphy by comparison with turbidite records from distal cores
Fluid escape features from MTD	Difficulties to assign stratigraphic level due to disturbed top reflections	Uncertainty in the assignment of the stratigraphic level	Study the thinner/distal parts of the MTD where fluid escape features are smaller/absent
Landslide erosion	- Hiatus in age-depth model - Obliterating evidence for older MTDs of smaller extent	- Unreliable age-depth model when erosion is undetected - Underrepresentation of the presence and/or impact of older events	- More dates needed near hiatus for age-depth model - Study most distal parts of MTD where erosion is absent: estimate hiatus size
Operator subjectivity "Wishful thinking"	Wrongly assigning MTD to a level of multiple MTDs → Less event horizons detected than present in the data	Underrepresentation of the number of paleoseismic events	- Independent analysis by multiple operators - Development of strict guidelines for MTD mapping

The subaqueous landslide cycle in south-central Chilean lakes: the role of tephra, slope gradient and repeated seismic shaking

Moernaut, J., Van Daele, M., Heirman, K., Wiemer, G., Molenaar, A., Vandorpe, T., Melnick, D., Hajdas, I., Pino, M., Urrutia, R., De Batist, M.

Supplementary figures

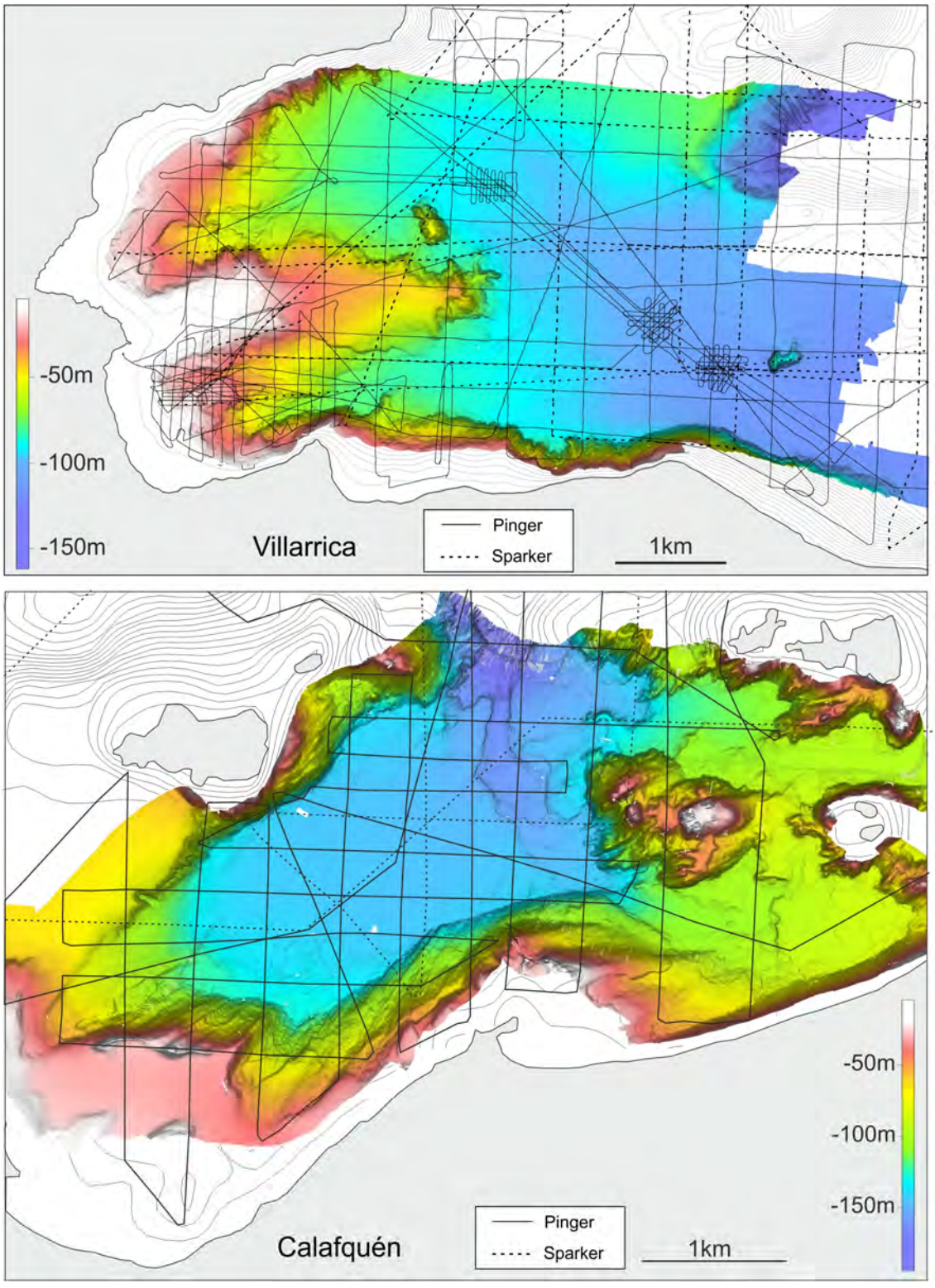

Si-Fig. 1: Reflection seismic survey grids in lakes Villarrica (above) and Calafquén (below) on the multibeam bathymetry maps. Details of the pinger and sparker systems can be found in section 3.

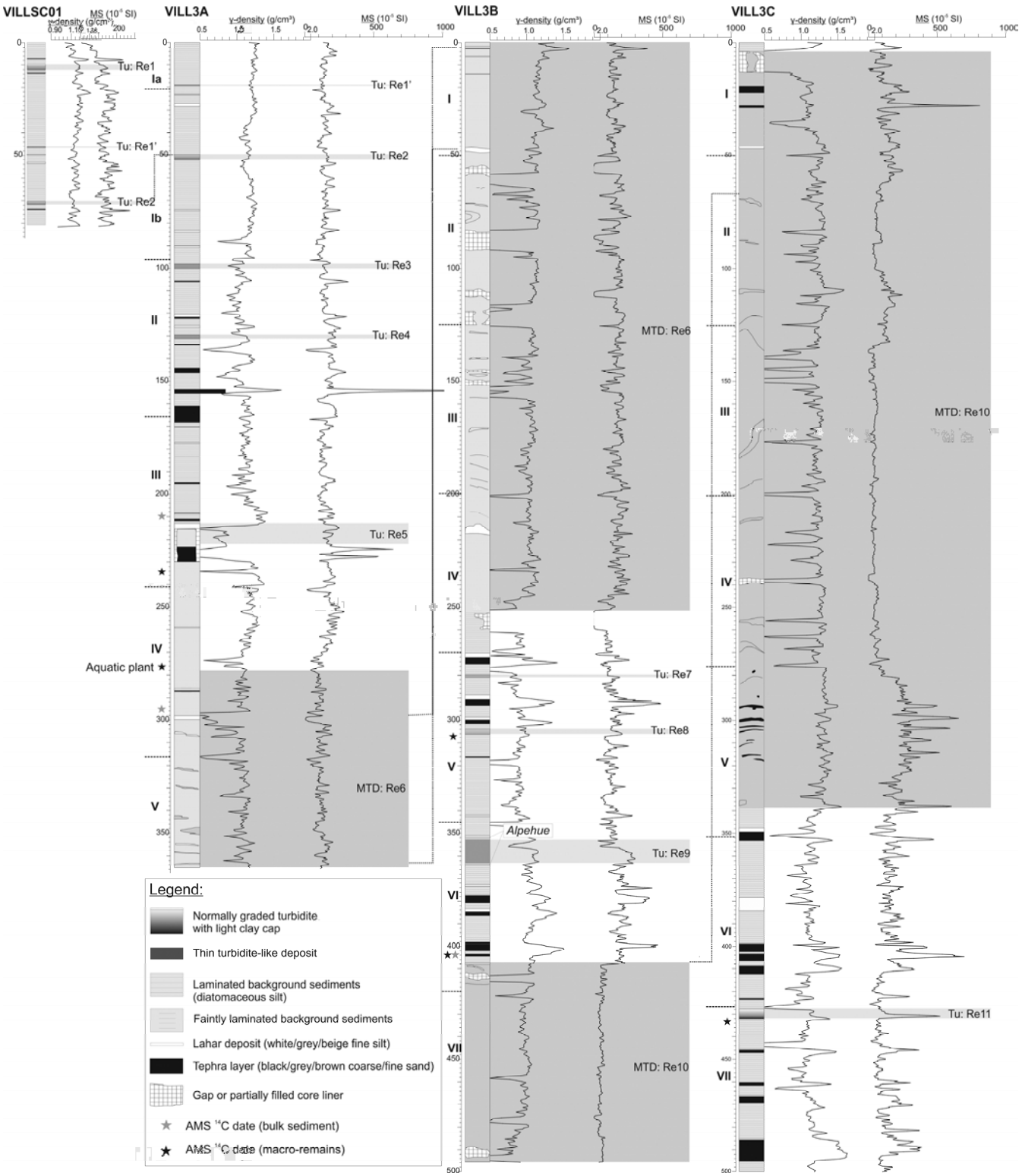

Si-Fig. 2: Detailed lithological log of the core segments of VILL3 (see legend) with indication of magnetic susceptibility, γ-density and locations of radiocarbon samples. Troughs in γ-density are caused by cracks in the sediments and partly-filled liners. Peaks in MagSus are associated with deposits of volcanic origin (tephra, lahars) or with a thin sandy base of lacustrine turbidites (Tu).

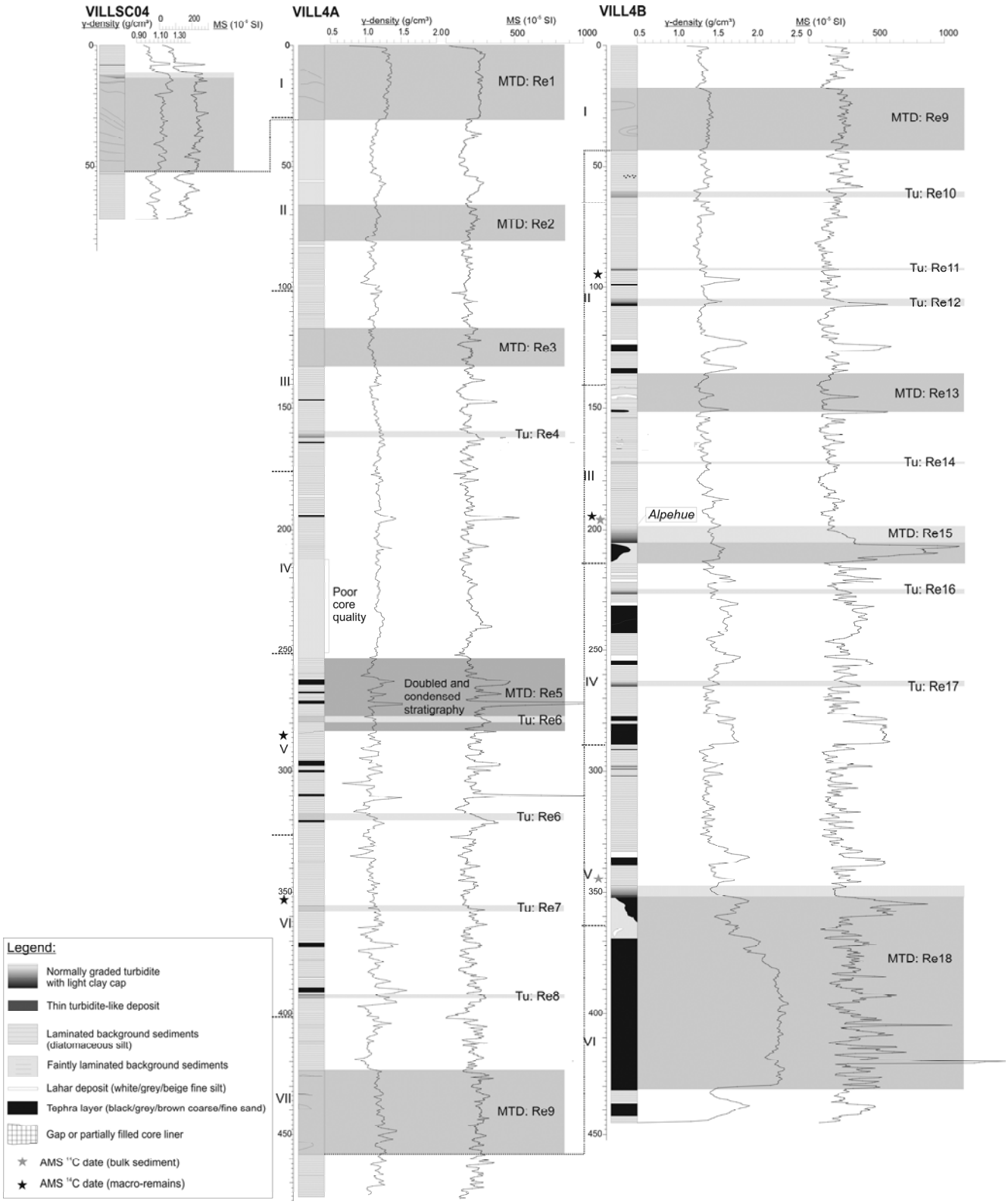

Si-Fig. 3: Detailed lithological log of the core segments of VILL4 (see legend) with indication of magnetic susceptibility, γ-density and locations of radiocarbon samples. Troughs in γ-density are caused by cracks in the sediments and partly-filled liners. Peaks in MagSus are associated with deposits of volcanic origin (tephra, lahars) or with a thin sandy base of lacustrine turbidites (Tu).

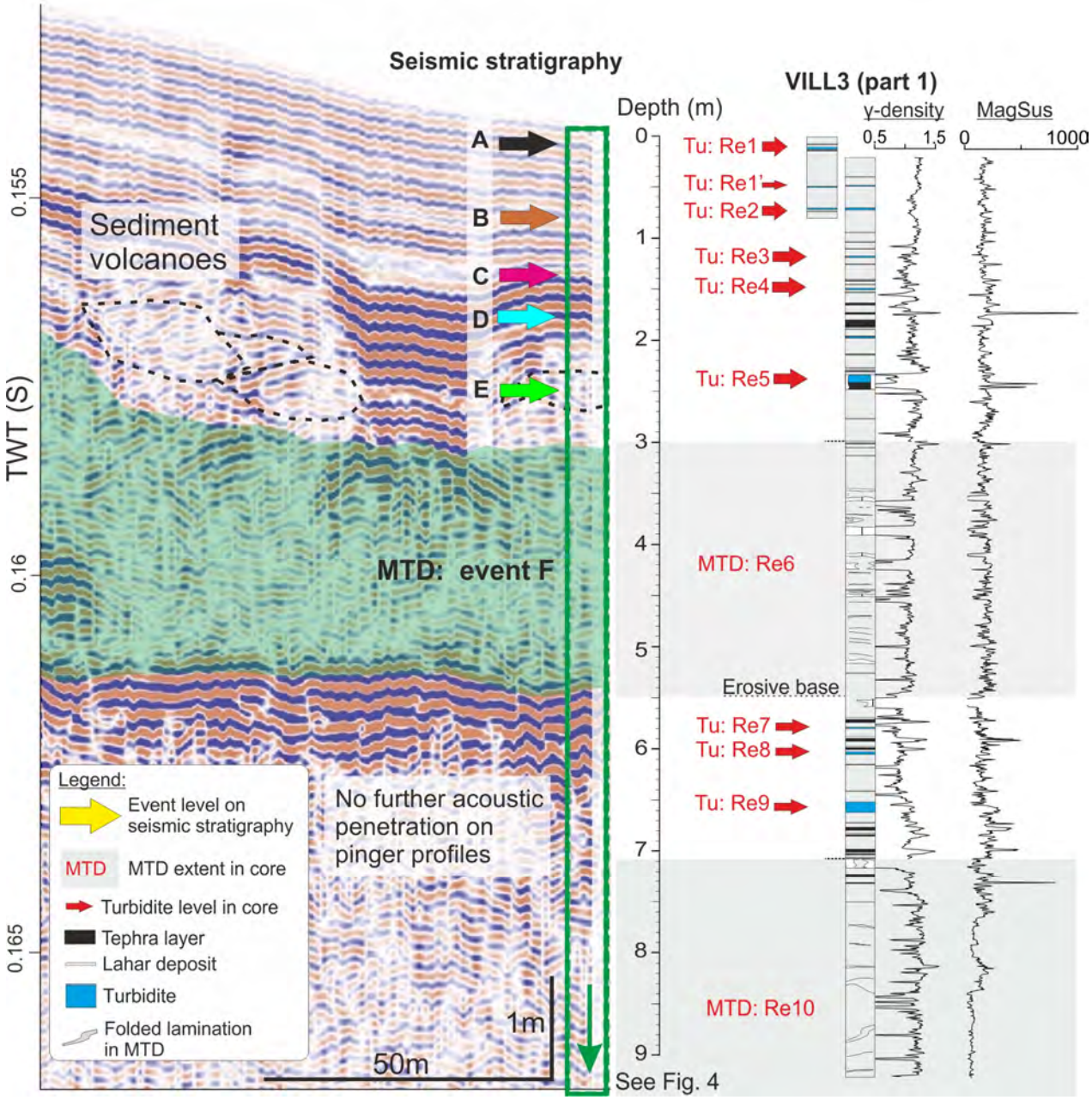

Si-Fig. 4: A) Core-to-seismic correlation of core VILL3 (upper 9 m) to a pinger profile. The MTD events on the seismic stratigraphy are shown as letters and colored arrows, the turbidites and MTDs in the cores as numbers. The values of γ-density are in g/cm^3 and those of magnetic susceptibility (MagSus) in 10^{-5} SI. The full core log and detailed legend of VILL3 is presented in SI-Fig. 2.

The subaqueous landslide cycle in south-central Chilean lakes: the role of tephra, slope gradient and repeated seismic shaking

Moernaut, J., Van Daele, M., Heirman, K., Wiemer, G., Molenaar, A., Vandorpe, T., Melnick, D., Hajdas, I., Pino, M., Urrutia, R., De Batist, M.

Supplementary tables: captions

Si-Table 1: AMS ^{14}C ages measured on cores VILL1, VILL3 and VILL4, with their corresponding stratigraphic depth (including and excluding event deposits), dated material and offset correction (if applicable) based on varve ages or paired dating of bulk sediments and macrofossils. Age information on CAL1 can be found in Moernaut et al. (2018).

Si-Table2: Comparison of obtained ages for seismic-stratigraphic levels in Lake Villarrica, based on the age-depth models of VILL1, VILL3 and VILL4. Only “best” ages are presented (i.e. weighted mean age).

SI Table 1

Core site	Core segment	Segment depth (cm)	Core depth (cm)	Event-free depth (cm)	^{14}C age (yr BP)	Error (yr)	Institute	Material	Offset correction (^{14}C yr)	Remarks
VILL1	VSC01	0.5	0.5	0.5	225	100	Poznan	Bulk	688	
VILL1	VILLSC02	68.5	68.5	67.7	720	25	NOSAMS	Macro-remains	0	paired
VILL1	VILLSC02	68.5	68.5	67.7	1360	25	NOSAMS	Bulk	688	paired
VILL1	VILL1-TEST-I	59.5	98	96.6	2350	30	NOSAMS	Bulk	688	
VILL1	VILL1-TEST-I	73.5	112	110.6	2600	30	Poznan	Bulk	688	
VILL1	VILL1-TEST-II	49.5	170.1	165.6	2670	35	NOSAMS	Bulk	688	
VILL1	VILL2B-I	102.5	287.75	280.85	3160	35	NOSAMS	Bulk	688	
VILL1	VILL1C-I	106.5	391	380.3	4140	40	NOSAMS	Bulk	688	
VILL1	VILL1C-II	56.5	447.8	433.3	4380	35	NOSAMS	Bulk	688	
VILL1	VILL1D-I	66.5	601.95	512.25	4530	30	NOSAMS	Bulk	688	
VILL1	VILL2D-II	57.5	754.95	661.35	6620	35	NOSAMS	Bulk	688	
VILL1	VILL1E-I	12.5	767.15	673.55	4445	35	Poznan	Macro-remains	0	paired
VILL1	VILL1E-I	12.5	767.15	673.55	5260	45	NOSAMS	Bulk	688	paired
VILL1	VILL1E-II	32.5	878.35	783.25	5290	50	NOSAMS	Bulk	688	
VILL1	VILL1E-II	93.5	939.35	841.15	5450	90	Poznan	Bulk	688	
VILL1	VILL1F-I	89.5	1039.4	940.1	6560	45	NOSAMS	Bulk	688	
VILL1	VILL1G-I	7.5	1196.45	1093.35	7370	45	NOSAMS	Bulk	688	
VILL1	VILL1G-II	93.5	1374.55	1268.05	9330	110	Poznan	Bulk	688	
VILL3	VILL3A-III	46	221.5	199.2	2400	45	NOSAMS	Bulk	688	
VILL3	VILL3A-III	69.5	255.1	208.1	2310	54	ETHZ	Macro-remains	0	
VILL3	VILL3A-IV	35	295.7	248	2825	26	ETHZ	Macro-remains (aqu	688	aquatic plant
VILL3	VILL3A-IV	55.5	316.2	xx	2980	35	NOSAMS	Bulk	688	in MTD
VILL3	VILL3B-V	36.5	612.6	291.1	2023	26	ETHZ	Macro-remains	0	
VILL3	VILL3B-VI	59.5	710.7	363.6	3070	30	ETHZ	Macro-remains	0	Paired
VILL3	VILL3B-VI	59.5	710.9	363.6	3680	45	NOSAMS	Bulk	688	Paired
VILL3	VILL3C-VII	7	1141.5	432.8	3653	61	ETHZ	Macro-remains	0	
VILL3	VILL3B-VI	6	656.7	333.8	x	x	x	Alpehue tephra	x	2951+-53 cal yr BP (Fontijn et al., 2016)
VILL4	VILL4A-V	34	307.4	196	1213	55	ETHZ	Macro-remains	0	
VILL4	VILL4A-VI	28	376.5	255.9	1774	57	ETHZ	Macro-remains	0	
VILL4	VILL4B-II	29.5	531.9	360.9	2293	70	ETHZ	Macro-remains	0	
VILL4	VILL4B-III	54.5	631.9	430.1	2138	45	ETHZ	Macro-remains	0	
VILL4	VILL4B-III	56	633.5	431.6	3370	45	NOSAMS	Bulk	688	
VILL4	VILL4B-V	54	780.6	519.1	3380	35	NOSAMS	Bulk	688	
VILL4	VILL4B-III	57	634.5	432.7	x	x	x	Alpehue tephra	x	2951+-53 cal yr BP (Fontijn et al., 2016)

SI Table 2

MTD level	"Best" Age via VILL1 (yr BP)	"Best" Age via VILL3 (yr BP)	"Best" age via VILL4 (yr BP)	Final "Best" age (yr BP)	Method
A	89	-3	8	-10	historical event
B	354	385	437	375	historical event
D	1740	1051	1136	1309	average VILL1-3-4
F	2225	2086	1928	2080	average VILL1-3-4
G	3128	2836	2371	2778	average VILL1-3-4
H	3448	2960	2621	3010	average VILL1-3-4
I	3812	3236	3040	3363	average VILL1-3-4
J	4314	3894	x	3894	VILL3
K	4821	x	x	4821	VILL1
L	5380	x	x	5380	VILL1
M	5991	x	x	5991	VILL1

Fluid escape levels without mapped MTDs	"Best" Age via VILL1 (yr BP)	"Best" Age via VILL3 (yr BP)	"Best" age via VILL4 (yr BP)	Final "Best" age (yr BP)	Method
C	1567	802	865	1078	average VILL1-3-4
E	2094	1687	1756	1846	average VILL1-3-4